https://doi.org/10.5194/acp-2021-927
Preprint. Discussion started: 11 January 2022


Atmospheric Chemistry and Physics Discussions

# The influence of multiple groups of biological ice nucleating particles on microphysical properties of mixed-phase clouds observed during MC3E

Sachin Patade[1*], Vaughan T. J. Phillips[1], Deepak Waman[1], Akash Deshmukh[1], Ashok Kumar Gupta[2], Arti Jadav[1], Aaron Bansemer[4], Jacob Carlin[3], Alexander Ryzhkov[3],

[1]Department of Physical Geography and Ecosystem Science, Lund University, Lund, Sweden

[2]Department of Earth and Environmental Sciences, Vanderbilt University, Nashville, TN, 37240, USA

[3]Cooperative Institute for Severe and High-Impact Weather Research and Operations, The University of Oklahoma, and NOAA/OAR National Severe Storms Laboratory, Norman, Oklahoma, USA

[4]National Center for Atmospheric Research, Boulder, Colorado, USA

*** Corresponding Author**

**Dr. Sachin Patade, Lund University, Sweden**

**email: sachin.patade@nateko.lu.se**

https://doi.org/10.5194/acp-2021-927
Preprint. Discussion started: 11 January 2022


**Abstract:**

A new empirical parameterization (EP) for multiple groups of primary biological aerosol particles (PBAPs) is implemented in the aerosol cloud model (AC) to investigate their roles as ice-nucleating particles (INPs). The EP describes the heterogeneous ice nucleation by (1) fungal spores, (2) bacteria, (3) pollen, (4) detritus of plants, animals, and viruses, and (5) algae. Each group includes fragments from the originally emitted particles. A high-resolution simulation of a midlatitude mesoscale squall line by AC is validated against airborne and ground observations.

Sensitivity tests are carried out by varying the initial vertical profiles of the loadings of individual PBAP groups. The resulting changes in warm and ice microphysical parameters are investigated. Overall, PBAPs have little effect on the ice phase, especially in the convective region. In the stratiform region, increasing the initial PBAP loadings by a factor of 100 resulted in less than 60% change in ice number concentrations. The total ice concentration is mostly controlled by various mechanisms of secondary ice production (SIP). However, when SIP is artificially prohibited in sensitivity tests, increasing the PBAP loading by a factor of 100 has no significant effect on the ice phase. Further sensitivity tests revealed that PBAPs have little effect on surface precipitation as well as on shortwave and longwave flux.

https://doi.org/10.5194/acp-2021-927
Preprint. Discussion started: 11 January 2022

Atmospheric Chemistry and Physics Discussions
Open Access
EGU

# 1. Introduction

In most climate models, the largest source of uncertainty for estimating the total anthropogenic forcing is associated with cloud-aerosol interactions (Forster et al., 2007). Atmospheric aerosol particles can act as cloud condensation nuclei (CCN) and a few of them act as ice-nucleating particles (INPs), thereby influencing the microphysical properties of clouds and, depending on the cloud-type, potentially affecting precipitation formation. This control of average cloud particle sizes regulates the radiative properties of layer clouds produced in convection possibly influencing the atmospheric radiation budget. Various sources of aerosol particles, including dust/metallic, marine aerosols, anthropogenic carbonaceous emissions, and primary biological aerosol particles (PBAPs), contribute to the observed INPs.

The formation of most precipitation globally is associated with the ice phase in cold clouds (Heymsfield and Field 2015). In particular, mixed-phase clouds are vital for the global climate. In a multimodel simulation study, Tsushima et al. (2006) showed that the doubling of $CO_2$ concentrations caused the changes in the distribution of cloud-water in the mixed-phase clouds in a climate simulation to be significant. Mixed-phase clouds play an important role (about −3.4 $Wm^{-2}$) in the global net cloud radiative forcing of the present-day climate (e.g., Matus and L'Ecuyer 2017).

PBAPs are solid particles containing insoluble material of biological origin and are emitted from the Earth's surface.  They are highly active in initiating ice as INPs and include bacteria, fungal spores, pollen, algae, lichens, archaea, viruses, and biological fragments (e.g., leaf litters, insects) and molecules (e.g., proteins, polysaccharides, lipids). Considering the onset

https://doi.org/10.5194/acp-2021-927
Preprint. Discussion started: 11 January 2022




temperature of freezing, some ice nucleation active fungi and bacteria (especially *Pseudomonas syringae*) are among the most active INPs present in the atmosphere (Després et al. 2012; Hoose and Möhler 2012). The potential impact of PBAP INPs on cloud microphysical characteristics has been recognized for many years. However, this topic remains a subject of debate. Some previous modeling studies have shown that on a global scale PBAPs have only a limited influence on clouds and precipitation (Hoose et al. 2010; Sesartic et al. 2012, 2013; Spracklen and Heald 2014). On a global scale, the percentage contribution of PBAPs to the immersion freezing is predicted to be much smaller (0.6%) as compared to dust (87%) and soot (12%) (Hoose et al. 2010).

Many studies have used cloud models to highlight the potential impact of PBAP INPs on cloud microphysics and precipitation (e.g., Levin et al. 1987; Grützun et al. 2008; Phillips et al. 2009; Hummel et al. 2018). For example, the mesoscale aerosol-cloud model by Phillips et al. (2009) had a 3-D domain of about 100 km in width, and many cloud types were present in the mesoscale convective system that was simulated. Their simulations revealed that the cloud cover, domain radiative fluxes, and surface precipitation rate were significantly altered by boosting organic aerosols representing PBAPs. According to Hummel et al. (2018) in shallow mixed-phase clouds (i.e., altostratus) when the cloud top temperature is below -15ºC, PBAPs have the potential to influence the cloud ice phase and produce ice crystals in the absence of other INPs.

The quest for insights about the broader atmospheric role of PBAP INPs for cloud microphysical properties and precipitation is hampered by the limited availability of observations both of their ice nucleation activities for various species and their aerosol

https://doi.org/10.5194/acp-2021-927
Preprint. Discussion started: 11 January 2022




distributions in the real atmosphere. More generally, there is incomplete knowledge about the chemical identity of the key INPs, whether biological or otherwise (Murray et al. 2012). In many global and regional models, the ice nucleation activity of bioaerosols is represented either empirically or theoretically based on laboratory measurements of specific biological species of PBAPs that are assumed as representative candidates (e.g., *Pseudomonas syringae*). This assumption of representativeness introduces uncertainties that would be expected to impact the model results, potentially introducing a bias into the estimation of effects of bioaerosols on clouds.

In addition to primary ice nucleation, ice formation in clouds can occur because of processes generating new particles from pre-existing ice, and these are known as Secondary Ice Production (SIP) mechanisms. SIP can have a considerable impact on cloud micro- and macro-physical properties such as precipitation rate, glaciation time, cloud lifetime, and cloud electrification by modifying the order of magnitude of ice particle concentrations (e.g., Blyth and Latham (1993); Crawford et al., 2012; Lawson et al., 2015; Phillips et al., 2017b, 2018, 2020; Phillips and Patade, 2021; Sotiropoulou et al. 2021a,b). This in turn can influence the global hydrological cycle and climate. For example, Zhao and Liu (2021) demonstrated using a global climate model that SIP dominates ice formation in moderately cold clouds and has a significant influence on their liquid and ice water paths. They showed that including three SIP mechanisms in the model simulated global annual average liquid water path decreases by $-15$ g m$^{-2}$ ($-22$%) and the ice water path increases by 9 g m$^{-2}$ (23%), resulting in better agreement with observations. Accounting for SIP in their model results in a change in the global annual average net cloud radiative forcing by about 1 W m$^{-2.}$ Although this is a small fraction of the total cloud radiative forcing globally, this flux change underlines the ubiquitous role of SIP on cloud properties on the large scale.

https://doi.org/10.5194/acp-2021-927
Preprint. Discussion started: 11 January 2022




However, in many cloud models, the representations of these SIP mechanisms are uncertain. A few secondary ice formation processes (e.g., Hallet-Mossop, 1974) have been suggested to be active in the temperature range where active PBAP INPs exhibit strong ice nucleation activity. The INPs of biological origin such as bacteria are highly active in the temperature range of the Hallet-Mossop (HM) process (-3 to -8ºC) as compared with non-biological INPs (Möhler et al. 2008; Patade et al., 2021). At temperatures warmer than -15°C, some of the PBAPs generated by biologically active landscapes can promote ice formation and crystal growth in clouds (Morris et al., 2014).

In the USA, about 18% of the total landmass is used as cropland, farmland, and agricultural activities. These are major sources of biological particles in the atmosphere. Biogenic particles released from crops, either pre- and post-harvest, have previously been shown to serve as INPs (in Colorado and Nebraska, (Garcia et al. 2012). Huffman et al. (2013) found that airborne biological particles increase significantly in concentration, by an order of magnitude or more, during rainfall in a forest in the western US and that bioaerosols are well correlated with INPs. Prenni et al. (2013) observed a similar increase in concentrations of ground-level INPs during rain at a forested site in Colorado, which was associated with increased biological particles. If these potential INPs are detrained from the convective outflow of a cell at mid-levels, then they may be entrained into other clouds aloft, influencing the microphysical properties of that subsequent storm. Convective clouds can efficiently transport lower tropospheric aerosol particles into the upper troposphere where they can affect the cloud properties (Cui and Carslaw, 2006)

https://doi.org/10.5194/acp-2021-927
Preprint. Discussion started: 11 January 2022




The current study aims to simulate realistic concentrations of multiple groups of PBAP INPs, including bacterial and fungal particles, to investigate their interactions with convective clouds observed during the Midlatitude Continental Convective Clouds Experiment field campaign (MC3E), (Jensen et al. 2016), in the USA. In view of the literature noted above about effects from PBAP INPs, there is a need for more detailed analyses of their role in altering cloud microphysical properties and precipitation because the realistic treatment of IN activity for major PBAP groups was not available, prior to our empirical scheme (Patade et al. 2021). Hitherto, laboratory measurements of isolated biological species (e.g., *Pseudomonas syringae*, *Cladosporium sp*) have been the basis for attempts to simulate biological ice nucleation in clouds, but the representativeness of the choice of such species has been a longstanding issue. It is not known which biological species of INA PBAPs contribute the most to biological ice nucleation. Consequently, there is a need for a new approach oriented toward laboratory measurements of natural biological INPs sampled from the real atmosphere, thus optimizing the representativeness of the data for studies of natural clouds.

In this paper, such an approach is followed to investigate the effect on cloud properties from various major groups of PBAP. We incorporated a recent empirical parameterization for various PBAP groups by Patade et al. (2021, henceforth PT21) into our 3D aerosol-cloud model (AC). PT21 created an empirical formulation resolving the ice nucleation of each group of PBAPs including 1) fungal spores and their fragments, 2) bacteria and their fragments, 3) pollen and their fragments, 4) detritus of plants, animals, and viruses, and 5) algae.

https://doi.org/10.5194/acp-2021-927
Preprint. Discussion started: 11 January 2022




The paper is structured as follows. In the next two sections, the methodology for the model setup and a description of the observed storm simulated. The subsequent section shows results comparing simulated cloud properties with observations to validate the model. There follows the analysis of sensitivity tests concerning the loading of PBAPs. In this article, we also examine the relative importance of various secondary ice processes in their role in mediating the PBAP effects on cloud microphysical properties, given the weakness of PBAP effects on cloud microphysical properties.

## 2. Description of field campaign of observations

### *2.1 Selected case of a deep convective system*

In the current study, we simulated a squall line that occurred on 20 May 2011 MC3E (Jensen et al. 2016). The MC3E campaign took place from 22 April through to 6 June 2011 and was centred at the Atmospheric Radiation Measurement (ARM) Southern Great Plains (SGP) Central Facility (CF), (36.6◦N, 97.5◦W) in north-central Oklahoma. Jensen et al. (2016) describe the squall line as a "golden event" of the MC3E campaign in view of the robust *in situ* sampling of extensive stratiform outflow from deep convection on this day. The surface meteorological analysis on 20 May indicated a southerly flow at the surface, which provided enough moisture from the Gulf of Mexico to trigger convection. Deep convection, organized in the form of a squall line, passed over the measurement site between 1030 and 1100 UTC, resulting in convective precipitation. It was followed by widespread stratiform precipitation that was well observed by both airborne and ground-based measurements.

https://doi.org/10.5194/acp-2021-927
Preprint. Discussion started: 11 January 2022


The skew-*T* plot from the radiosonde sounding conducted on 20 May 2011, at (00 UTC) is shown in Figure 1. The skew-T plot shows that the surface-based Convective Available Potential Energy (CAPE) for this case was 2355 J $kg^{-1}$, and the Lifting Condensation Level (LCL) was located at 840 hPa. The temperature at LCL, which is generally at the same height as the convective cloud base, was 14°C. The estimated amount of vapour in the entire depth of the troposphere corresponded to precipitable water of 3 cm.

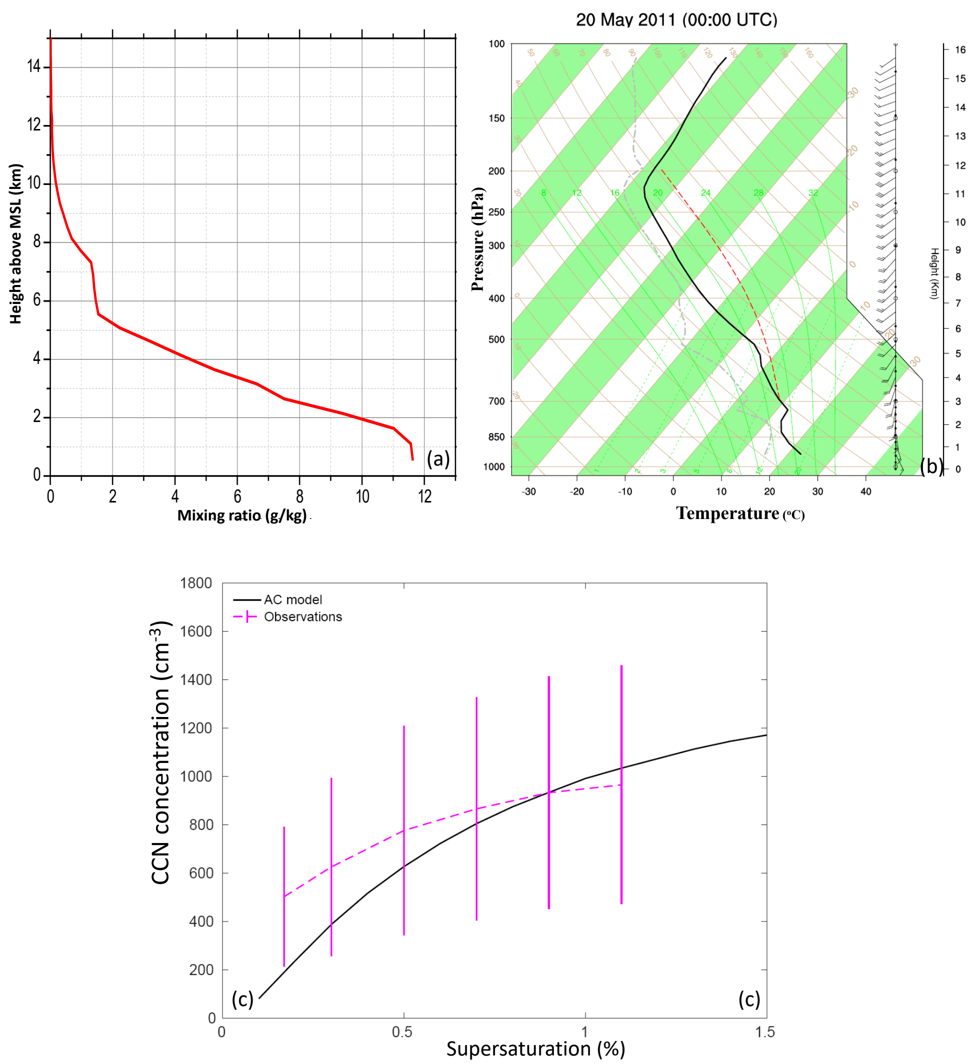

https://doi.org/10.5194/acp-2021-927
Preprint. Discussion started: 11 January 2022




**Figure 1.** (a) Vertical profile of water vapor mixing ratio on 20 May 2011 at 00 UTC. (b) The *skew T* plot from May 20, 2011, sounding. The air temperature is represented by the solid black line, while the dew point temperature is represented by a dashed grey line. The moist adiabat is represented by a dotted red line. (c) The CCN spectrum from AC for a simulated squall line case on May 20, 2011, for an environment 500 meters above MSL. The predicted CCN spectrum is compared to the observed CCN spectrum at the SGP CF (300 m above MSL).

### *2.2 Aircraft Observations*

The *in situ* microphysical observations used in this study were obtained from a University of North Dakota Citation II aircraft. The aircraft collected observations of cloud microphysical parameters from cloud base (1.8 km above MSL) to a maximum altitude of 7.5 kilometres above MSL. The MC3E campaign collected extensive airborne measurements of aerosols and cloud microphysical properties over north-central Oklahoma. A detailed description of the scientific objectives of the MC3E program, including the field experiment strategy, airborne and ground-based instrumentation, is given in the paper by Jensen et al. (2016). This section summarizes the instrumentation used in the current study.

**Table 1:** Details of aircraft instruments used in this study.

| **Instrument** | **Measurement** | **Typical range** |
|---|---|---|
| Cloud imaging probe (CIP) by Droplet Measurement Technologies (DMT) | Size distribution of cloud and precipitation particles | 0.025–1.5 mm (0.2-1 mm for model validation in the current study) |
| 2D cloud imaging probe (2D-C) | Size distribution of cloud and precipitation particles | 0.03–1.0 mm (0.2-1 mm for model validation in the current study) |
| Cloud droplet probe (CDP) | Cloud droplet spectra | 2–50 µm |
| High-volume precipitation spectrometer, version 3 (HVPS-3) | Precipitation particle spectra | 0.15–19.2 mm |

https://doi.org/10.5194/acp-2021-927
Preprint. Discussion started: 11 January 2022



| | | |
|---|---|---|
| King hot-wire liquid water content (LWC) probe | Cloud liquid water | 0.01–5 g $m^{-3}$ |
| Temperature probe | Ambient air temperature | – |
| Static pressure sensor | Ambient air pressure | – |

The Citation aircraft was equipped with a standard suite of meteorological instruments, which provided high-resolution measurements of temperature, pressure, and humidity. In addition, it carried microphysical probes for cloud and precipitation, and liquid water content, as listed in Table 1.

Particle size distributions (PSDs) from cloud to precipitation particle sizes were measured with various probes, including a 2D Cloud Imaging Probe (2D-C), a Cloud Imaging Probe (CIP), and a High-Volume Precipitation Spectrometer Probe (HVPS). The 2D-C and CIP probe data were processed objectively using the algorithm developed at the National Center for Atmospheric Research (NCAR) to mitigate artifacts produced by shattering on the probes' leading edges (Field et al. 2006). The 2D-C probe was equipped with Korolev anti-shattering tips (Korolev et al., 2011), while the CIP did not have anti-shattering tips. The size distribution of cloud drops with diameters from 2 to 50 μm was measured using a Cloud Droplet Probe (CDP). A King hot-wire liquid water content (LWC) probe measured the LWC. Vertical velocity is derived from air motion sensing systems available on the research aircraft.

*2.3 Ground-based measurements*

https://doi.org/10.5194/acp-2021-927
Preprint. Discussion started: 11 January 2022




A comprehensive instrumentation suite deployed at the ARM-SGP central facility provided continuous measurements of atmospheric gases, aerosols, clouds, and local meteorological conditions (e.g., wind, temperature, precipitation, and atmospheric profiles). A cloud condensation nuclei (CCN) counter (DMT) measured the CCN number concentration at seven supersaturation values with a temporal resolution of 1 hour. Surface precipitation was measured with 16 rain gauge pairs placed within a 6-kilometer radius of the SGP CF.

During the MC3E campaign, the extended facility deployed at CF measured the spatial variability of surface fluxes of heat, moisture, and momentum. A radiosonde array of 6 sites, covering an area of 300 km × 300 km, was designed to capture the large-scale variability of the atmospheric state. Radiosonde observations (Vaisala RS92-SGP) were conducted four times daily at around 05:30, 11:30, 16:30, and 22:30 UTC, providing vertical profiles of atmospheric state variables (pressure, temperature, humidity, and winds) of the environment surrounding the ARM SGP site. When aircraft operations were planned based on forecasted convective conditions, the sounding frequency was increased to eight times per day.

In addition to airborne observations, the ARM heterogeneous radar network was used to conduct unique radar observations during the MC3E campaign. The information about various radar assets during MC3E is given by Jensen et al. (2016). The surface precipitation used for model validation in this study is a radar-based precipitation estimate as described by Giangrande et al. 2014. They used radar observations from the C-band and X-band scanning ARM precipitation radars (C-band Scanning ARM Precipitation Radar and X-band Scanning ARM Precipitation Radars, respectively) to estimate rainfall to within 100 km of the ARM

https://doi.org/10.5194/acp-2021-927
Preprint. Discussion started: 11 January 2022


Atmospheric Chemistry and Physics Discussions

facility in Lamont, Oklahoma. Their radar-based rainfall retrievals were in good agreement with observations with absolute bias less than 0.5 mm for accumulations less than 20 mm.

The Interagency Monitoring of Protected Visual Environments (IMPROVE) network stations close to the location of airborne observations provided ground-level measurements of various chemical species. These included carbonaceous compounds (black and organic carbon), salt, ammonium sulfate, and dust. The measurements of these aerosol species from various IMPROVE sites, including Ellis (36.08ºN, 99.93ºW), Stilwell (35.75ºN, 94.66ºW), and Wichita Mountains (34.73 ºN, 98.71ºW) sites in Oklahoma, were averaged to provide inputs to AC. Initial concentrations for the aerosol species of AC (10 species) including sulfate, sea salt, dust, black carbon, soluble organic, and insoluble organic (five groups of bioaerosols) were derived from the Goddard Chemistry Aerosol Radiation and Transport (GOCART) model (Chin et al. 2000). Profiles of aerosol mass concentration were scaled at all levels to match simultaneous measurements by IMPROVE. The prescribed mass mixing ratios of aerosol species in AC-based IMPROVE observations are enlisted in Table 2.

**Table 2:** The mass mixing ratio of aerosol species based IMPROVE observations which are used as input to AC.

| **Aerosol species** | **Mass mixing ratio ($\mu g/m^3$)** |
|---|---|
| $(NH_4)_2SO_4$ | 0.56 |
| Dust | 0.18 |
| Sea salt | 0.021 |
| Black carbon | 0.093 |
| Soluble organic carbon (80 % of TOC) | 0.45 |
| Insoluble organic carbon (20 % of TOC) | 0.18 |
| PBAPs (50% of Insoluble organic carbon) | FNG=0.036;<br>BCT=0.012;<br>PLN=0.028; |

https://doi.org/10.5194/acp-2021-927
Preprint. Discussion started: 11 January 2022




| | |
|---|---|
| | DTS=0.016; ALG=0.000022 |

## 3. Methodology

### *3.1 Model description*

The '*aerosol-cloud model*' (AC) used in this study is a cloud-resolving model (CRM) with a hybrid spectral bin/two-moment bulk microphysics, interactive radiation, and semi-prognostic aerosol schemes (Phillips et al. 2017a, 2020). The model predicts the mass and number concentrations for five types of hydrometeors: cloud liquid, cloud ice (or "crystals"), rain, graupel/hail, and snow. The mixing ratios of the total number and mass of all particles in each microphysical species are treated as model prognostic variables. AC treats all known microphysical processes such as droplet nucleation, ice initiation through primary and secondary processes, and growth processes such as deposition/sublimation of ice particles, condensation/evaporation of drops, freezing/melting, as well as coagulation by collisions between various hydrometeor types. Both cloud-base and in-cloud activation of aerosols to form cloud-droplets are treated explicitly, with the predicted in-cloud supersaturation resolved on the model grid being used to activate aerosols aloft. Bin-resolved size distributions of each aerosol species are predicted for the interstitial and immersed components of each aerosol species. Extra prognostic variables track the number of aerosols in each aerosol species that have been lost by INP and CCN activation.

Secondary ice formation is represented by four types of fragmentation:

https://doi.org/10.5194/acp-2021-927
Preprint. Discussion started: 11 January 2022




- breakup in ice–ice collisions (Phillips et al. 2017a, b),
- Hallett and Mossop (1974), rime splintering,
- fragmentation of freezing rain/drizzle by modes 1 and 2 (Phillips et al. 2018);
- and sublimation breakup (Deshmukh et al. 2021).

The empirical parameterization (EP) (Phillips et al. 2013) of heterogeneous ice nucleation treats all known modes of ice formation (deposition mode, condensation-/immersion-freezing, inside-out and outside-in contact-freezing) in terms of dependencies on the loading, size, and chemistry of multiple aerosol species. In the previous version of the EP, there were four species of INP aerosol. One of these was PBAP INPs. However, that version of the EP did not resolve the individual types of PBAP IN, which exhibit a wide range of ice-nucleating abilities. A recent study PT21 provided an empirical formulation for multiple groups of PBAP INPs based on field observations over central Amazon. In this study, we modified AC by implementing the recent empirical parameterization of PBAP INPs by PT21. A summary of their formulation is provided in section 3.2.

Cloud processes and rainfall formation have been detected using different radar variables, such as specific differential phase $K_{DP}$. Moisseev et al. (2015), for example, noted an increase in observed $K_{DP}$ because of aggregation. In addition, a few studies have hypothesized evidence of SIP via $K_{DP}$ (e.g., Sinclair et al. 2016; Kumjian and Lombardo 2017; Carlin et al. 2021). In this study, we attempted to detect secondary ice formation signatures by implementing $K_{DP}$ estimations into AC. Based on Ryzhkov et al. (2011), $K_{DP}$ values were estimated for various hydrometeor types, including cloud drops, raindrops, cloud ice, snow, and graupel (their equations 22, 23, 24, 26, and 29). The scattering amplitudes were calculated using the Rayleigh approximation. The $K_{DP}$ estimations are made for 0° elevation angle and S-band (radar wavelength of 11 cm). The equivalent volume diameter of the given hydrometeor was used for all calculations.

*3.2 Empirical formulation for PBAP INPs:*

The empirical formulation by PT21 for multiple groups of PBAPs including:- 1) fungal spores (FNG), 2) bacteria (BCT), 3) pollen (PLN), 4) viral particles, plant/animal detritus (DTS), 5) algae (ALG) and their respective fragments are implemented in AC. This formulation is based primarily on field observations over the central Amazon rainforest, with empirically derived dependencies on the surface area of each group (except algae) and it applies to the particles with diameters greater than 0.1 μm. The concentrations of algal particles at the Amazon Tall Tower Observatory (ATTO) site were much smaller than our detection threshold, so we could not use a similar empirical treatment for ALG. The frozen fraction for the algal particles (Diatom cell, T. pseudomonas) available in the literature is used to estimate INPs from ALG (Wilson et al. 2015). PT21 elaborate further.

*3.3 Model setup*

AC was driven by initial and evolving boundary data for meteorological conditions. The model simulations were carried out for a three-dimension domain of 80 km x 80 km domain with horizontal grid spacings of 2 km. In vertical, the model resolution was 0.5 km, and the model top was located at about 16 km. The lateral boundary conditions are doubly periodic on all sides of the domain. The large-scale forcing condition used for the simulation was derived using the constrained variational analysis (Xie et al. 2014; Jensen et al. 2016). The

https://doi.org/10.5194/acp-2021-927
Preprint. Discussion started: 11 January 2022



initial time of the simulations was at 1200 UTC on 19 May 2011 and all simulations were performed for 48 hours at a time step of 10 seconds.

The GOCART model (Chin et al. 2000) was used to initialize the seven chemical species associated with the EP. The data from the three IMPROVE sites mentioned above (Section 2.3) was used to rescale the mass concentration profiles at all levels so that they match the measurements. Table 2 lists the mass mixing ratios of various aerosol species after the corrections. The relative contribution of insoluble and soluble organic carbon to the total organic carbon (TOC) was assumed to be 20% and 80%, respectively by assuming a water-soluble fraction of 80% for carbonaceous aerosol (Phillips et al. 2017b). Due to a lack of observational data, it was parsimoniously assumed that 50% of the insoluble organics were biological in origin. The total PBAP loading was prescribed partly based on observations of insoluble organics and partly based on the assumed fraction. PT21's observations were used to calculate the relative contribution of various PBAP groups to insoluble organics. The parameters for the shape of PSD of each PBAP group (modal mean diameters, standard deviation ratios, and relative numbers in various modes) are prescribed based on observations from Amazon (PT21).

From these prescribed loadings of aerosol species, AC predicts their size distribution and hence the CCN activity spectrum. Using the initial sounding and aerosol profile, AC can predict the in-cloud size distribution of aerosols in each species as well as in-cloud supersaturation. To validate this prediction, Figure 1c shows the predicted CCN spectrum compared with observations from the CCN counter at the surface at the SGP site. During 19-20 May, the measured number concentration of active CCN at the SGP CF ranged from 400 to 3000 $cm^{-3}$ at 1% supersaturation (Fridlind et al. 2017). The measurements were made on 20 May before the start of the rain in clear air. The normalized CCN number concentrations at 1% supersaturation from observations and AC are ~ 1000 $cm^{-3}$ and ~ 940 $cm^{-3}$, respectively. Given the wide range of observed CCN concentrations at each supersaturation, the predicted and observed CCN activity spectra are in good agreement.

## 4. Results from control simulation and model validation

### *4.1 Overview of the control simulation*

An intense north-to-south oriented squall line moved over the ARM SGP CF on May 20, 2011, from 1100 to 1400 UTC (Sec. 2.1). The new version of AC simulated this case, after implementing the empirical formulation by PT21 for multiple groups of PBAP INPs ('control' simulation) (Sec. 3).

https://doi.org/10.5194/acp-2021-927
Preprint. Discussion started: 11 January 2022


Atmospheric Chemistry and Physics Discussions

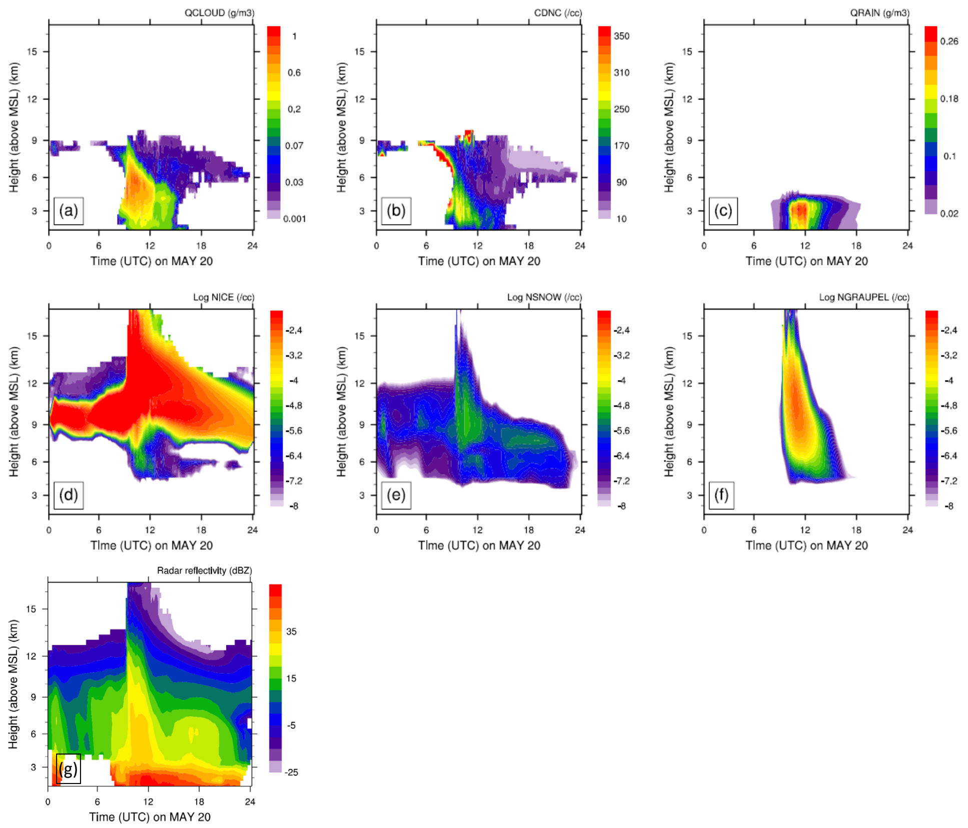


**Figure 2:** Time-height contours of domain averaged a) cloud water mixing ratio (QCLOUD); b) cloud droplet number concentration (CDNC); c) rainwater mixing ratio (QRAIN); d) number concentration of cloud ice (NICE); e) number concentration of snow (NSNOW); f) number concentration of graupel (NGRAUPEL). Due to a wide range of values, the log values number concentrations are plotted. The surface height is ~ 500 m. The averaging was done for cloud points with LWC > 0.001gm$^{-3}$ or TWC > 10$^{-6}$ gm$^{-3}$. Also shown is the time-height evolution of domain averaged (g) radar reflectivity.

Figure 2 shows the time-height evolution of various liquid and ice microphysical parameters derived from the control simulation conditionally averaged over cloudy regions. The maximum of the average cloud droplet number concentration was around 250 cm$^{-3}$. The liquid water content was typically less than 0.5 g m$^{-3}$. The freezing level (0ºC) was around 4.1 km above MSL. The deep convection began around 10 UTC, followed by intense

https://doi.org/10.5194/acp-2021-927
Preprint. Discussion started: 11 January 2022


precipitation around 11 UTC, and reached its peak around 12 UTC. The time-height evolution of cloud ice, snow, and graupel number concentrations shows maxima shortly before 12 UTC, which coincides with the time of peak precipitation. This suggests that the ice phase was important in precipitation formation.

The time-height map of simulated radar reflectivity during 20 May, unconditionally averaged over the whole domain is shown in Figure 2g. It shows the well-defined squall line passing over the domain from 1100 to 1500 UTC. The maximum of this domain-wide simulated reflectivity is around 40 dBZ (Fig. 2d) when deep convection was happening. The instantaneous maximum of reflectivity at any grid-point (not shown) was about 50 dBZ. At other times, the average reflectivity was typical of the stratiform cloud of about 15 dBZ. The cloud top height of the squall line decreases after 1400 UTC.

*4.2. Model validation against coincident observations of the storm*

The extended stratiform region of the squall line while in the vicinity of the SGP CF was sampled by the Citation aircraft equipped with a full suite of cloud microphysical instrumentation (Sec. 2). The aircraft started sampling the stratiform precipitation region at around 1300 UTC and continued the observations at sub-freezing temperatures from 1335 to 1515 UTC. Occasionally, the aircraft encountered weak convective updrafts (< 6 m/s). The aircraft actively avoided convection that was more vigorous than that. In this section, we validate various microphysical and dynamical quantities from the control simulation against aircraft and ground measurements.

https://doi.org/10.5194/acp-2021-927
Preprint. Discussion started: 11 January 2022



Figure 3 compares the aircraft observations against predicted microphysical quantities, with both the predictions and observations identically averaged, conditionally over convective (6 > |*w*| > 1 m/s) and stratiform regions |*w*| < 1 m/s). The simulated LWC decreases exponentially with height above cloud base. There is considerable scatter in observed LWC at each level. The various degrees of dilution of sampled parts of the cloud can cause these variations in LWC at a given altitude. The maximum simulated LWC of 0.5 $gm^{-3}$ was observed in the convective region at temperatures warmer than -5ºC. Overall, the means of observed LWC are in good agreement with the model results for convective as well as stratiform regions.

The vertical profiles of simulated and observed Cloud Drop Number Concentration (CDNC) (Fig. 3c and 3d) showed that CDNC was lower than 300 $cm^{-3}$. Overall, the mean values of CDNC simulated for convective and stratiform regions are in good agreement with observations. The observed and simulated mean diameter of cloud-droplets varied between 6 to 15 µm over height (Figure 3e and 3f). Overall, the predictions of average CDNC and cloud droplet diameter, in both convective and stratiform regions, show good agreement with observations.

https://doi.org/10.5194/acp-2021-927
Preprint. Discussion started: 11 January 2022

Atmospheric Chemistry and Physics
Discussions

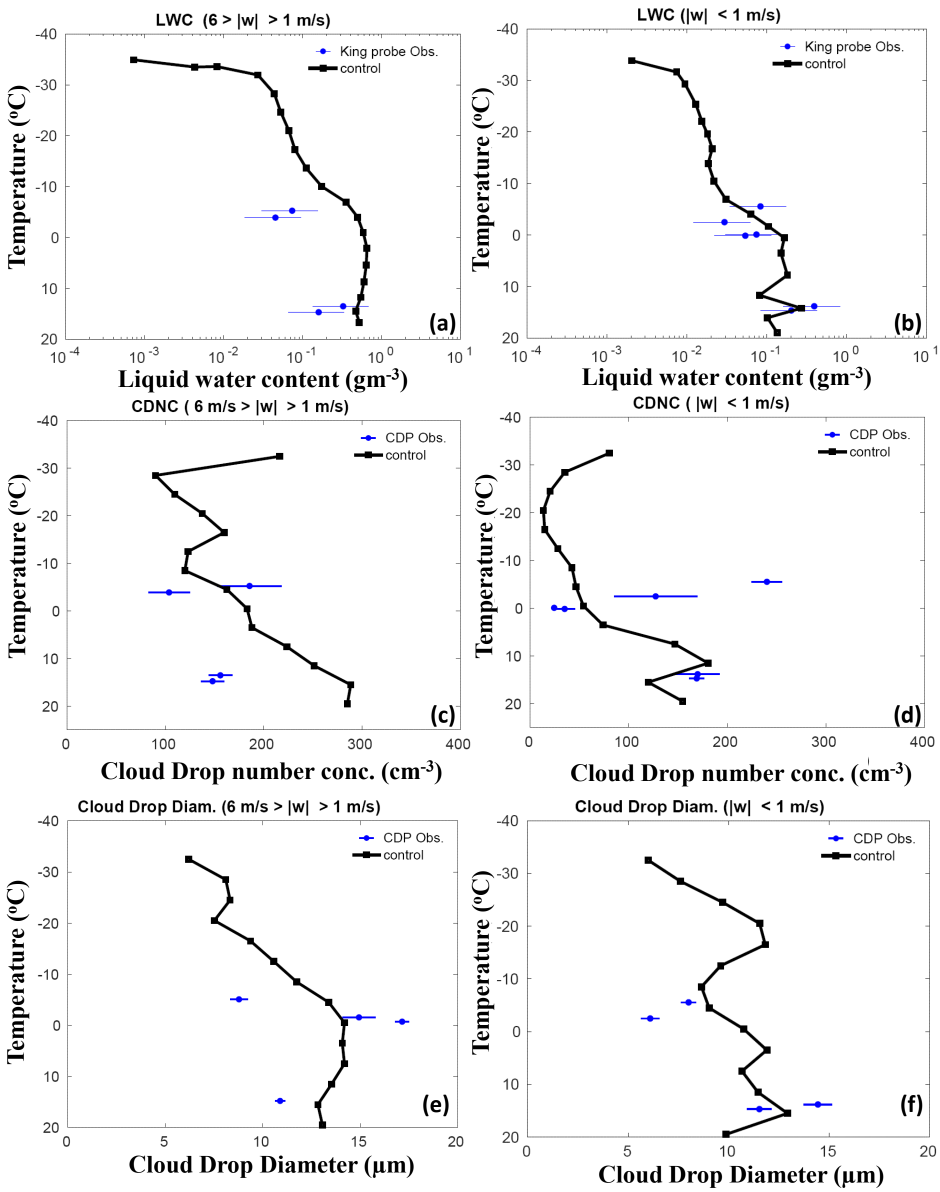


**Figure 3:** Comparison of the control simulations by AC with aircraft observations, for liquid water content conditionally averaged over (a) convective (6 m/s > |*w*| > 1 m/s) and (b) stratiform (|*w*| < 1 m/s) regions; cloud drop number concentration over (c) convective and (d) stratiform regions; average size of cloud droplets (< 20 $\mu$m) conditionally averaged over (e) convective and (f) stratiform regions. All the vertical profiles shown here are averaged for the whole domain.

https://doi.org/10.5194/acp-2021-927
Preprint. Discussion started: 11 January 2022

Atmospheric Chemistry and Physics Discussions

The ice particle number concentration from observations and the control simulation is also compared as shown in Figures 4a and 4b for convective and stratiform regions, respectively. Observations show that the concentration of ice particles gradually increases as the temperature decreases, as predicted. The maximum ice number concentration from the aircraft observations (with $D$ > 200 μm) is ~ 60 $L^{-1}$ around -15 ºC. The number concentrations of ice particles from the model with a diameter larger than 200 μm (cloud ice, snow, graupel) (denoted by 'NT200') is compared with observed ice number concentrations from CIP as well as from combined probes including 2DC, CIP, and HVPS. Ice particles smaller than 200 μm from these imaging probes were excluded due to difficulties in measuring small ice particles (Korolev et al., 1991) as well as to avoid contamination from large cloud droplets. Good agreement to within 50% at most levels, was found between the model simulated (NT200) and that observed for the convective region.

In the stratiform region, at most levels, model values of NT200 have the same order of magnitude as observations. However, between about the -10 and -16ºC levels, the stratiform NT200 values are about two-thirds of an order of magnitude lower than the observations. In similar simulations of the 20 May case, Fan et al. (2015) and Fridlind et al. (2017) also showed underestimation of measured ice number concentrations. Compared to observations, their simulations showed half an order of magnitude bias in ice crystal number concentration. Comparatively, our model predicted ice number concentrations were in better agreement with observations. As mentioned in section 2.2, imaging probe data is prone to shattering, and various corrections were used to rectify it. However, there are currently no ways to determine how many undetected artifacts remain after shattering corrections have been applied. Such

https://doi.org/10.5194/acp-2021-927
Preprint. Discussion started: 11 January 2022


Atmospheric Chemistry and Physics Discussions
Open Access

uncertainties in measured ice number concentration could result in such bias in observed and simulated ice number concentrations.

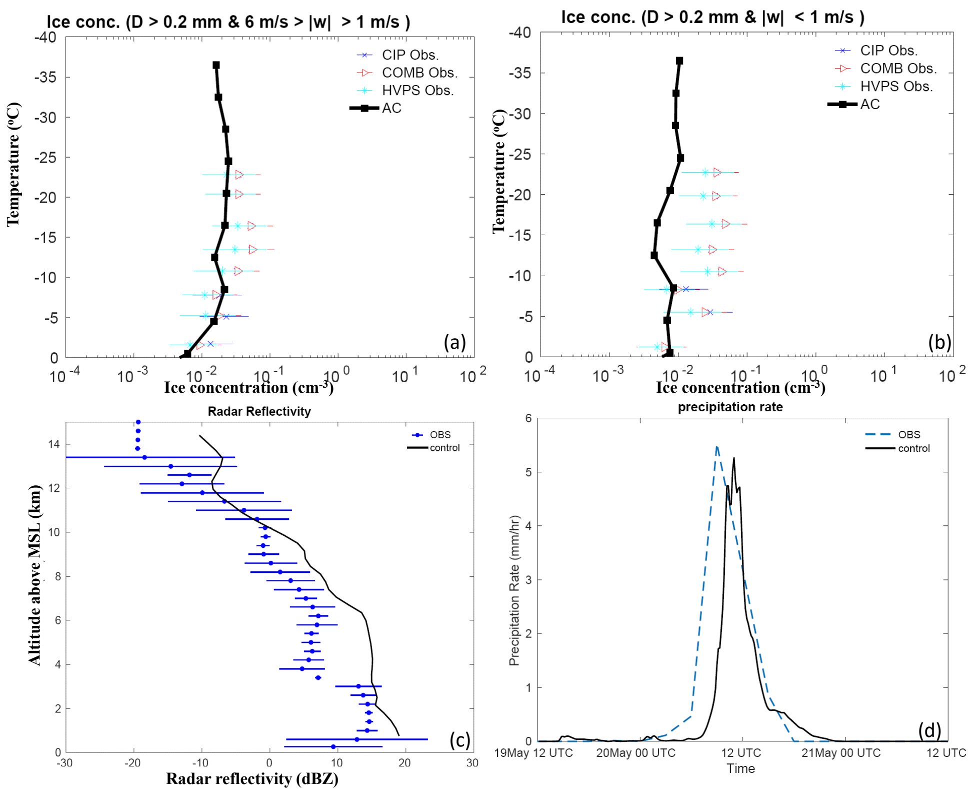


**Figure 4**: Comparison of the control simulations by AC with aircraft observations, for ice number concentration of all particles > 0.2 mm in the maximum dimension of all microphysical species (cloud ice, graupel/hail, snow), averaged over (a) convective (6 m/s > |*w*| > 1 m/s) and (b) stratiform (|*w*| < 1 m/s) regions. (c) The vertical profile of simulated radar reflectivity conditionally averaged over all regions of significant reflectivity (> -20 dBZ) at each level is compared with observations from ground-based radars. The temperature corresponding to each altitude is mentioned on the right axes; (d) predicted precipitation rate (mm/hr) compared with ground observations at the SGP CF. All the vertical profiles shown here are averaged for the whole domain.

https://doi.org/10.5194/acp-2021-927
Preprint. Discussion started: 11 January 2022




In Figure 4c, the radar reflectivity from vertically pointing Ka-band ARM zenith radar is compared with the mean profile from model simulations. This illustrates figure illustrates that simulated reflectivity profiles below roughly 3 km and above 8 km MSL altitudes are in good agreement with observations. Between 3 and 8 km MSL (temperatures of 2 and -30ºC), the bias in reflectivity from model simulations and observations is about 7-8 dBZ. Thus, the simulated reflectivity is substantially higher than observed, particularly at levels where the aircraft sampled the clouds. Fridlind et al. (2017), as well as Fan et al. (2015), noticed similar overestimations of reflectivity within stratiform outflow of the squall line case on 20 May. They attributed the reflectivity biases to significantly larger ice particles in the simulations than observed.

Figure 4d compares the time series of precipitation rate from the control simulation with the radar-based precipitation estimates. In both, control simulation and observations, a maximum precipitation rate of about 5 mm/hr was noticed, with an error in the prediction of less than 5%. In comparison to observations, the simulated squall line arrives 1-2 hours later. The lack of resolution of the 3D turbulence in the PBL and uncertainties associated with the 3D structure of initial and boundary conditions can all have an independent impact on the simulated rainfall structure, resulting in a delayed peak. Nonetheless, good agreement between predicted and retrieved precipitation rates is observed.

### *4.3 Analysis of simulation with ice particle budgets and tagging tracers*

The activated PBAP INPs from the budget of the control run are shown in Figure 5 for the convective and stratiform regions. Overall, bacterial, and fungal particles dominate the

https://doi.org/10.5194/acp-2021-927
Preprint. Discussion started: 11 January 2022


Atmospheric Chemistry and Physics
Discussions

biological INP concentration in the simulated cloud. For example, at -20ºC the activated INPs from bacteria and fungi are higher than the other three groups of PBAP INPs (detritus, pollen, algal) by two orders of magnitude in both convective as well as stratiform regions. At that level in convective regions, the maximum of the average concentration of simulated active PBAP INPs is about 0.003 L-1, which is two orders of magnitude less than the maximum total for all active INPs (about 0.3 L-1) in the whole simulation. In addition to the PBAP INPs, Figure 5 also shows the activated INPs from dust and black carbon. Overall, the predicted total INP concentration is dominated by black carbon and dust. At -10ºC, the Activated INPs from dust and black carbon differ by an order of magnitude from the total PBAP INPs in convection.

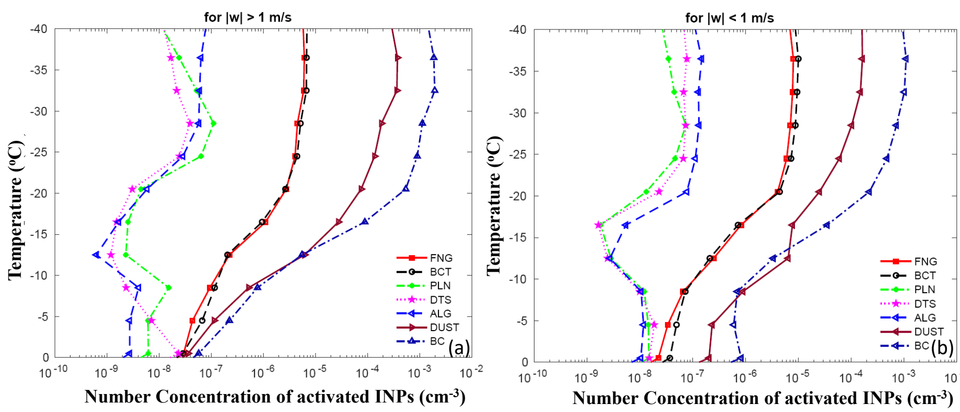


**Figure 5:** The activated number concentration INPs from various PBAP groups along with dust (DUST) and black carbon (BC) at various temperatures for (a) convective and (b) stratiform regions. All the vertical profiles shown here are averaged for the whole domain.

The formation of ice in a cloud is a result of several primary and secondary processes. It is important to understand the relative importance of these processes in precipitation formation.

https://doi.org/10.5194/acp-2021-927
Preprint. Discussion started: 11 January 2022

Atmospheric Chemistry and Physics
Open Access
EGU
Discussions

To that end, in Figure 6a a budget is provided for the total numbers of all ice particles initiated from various sources throughout the 3D domain of the entire simulation.

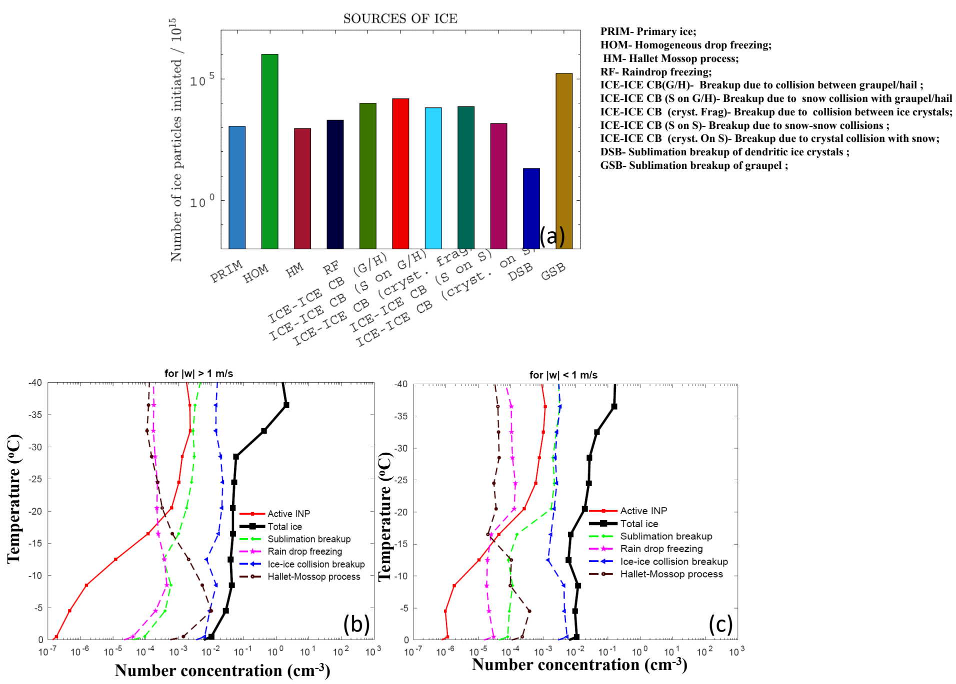


**Figure 6:** (a) Ice crystal budget for simulated MC3E case. The number of ice crystals produced by various mechanisms (as shown in the legend box) per $10^{15}$ particles is shown. The number concentration of ice particles from the model is shown for the whole range. Also shown is the number concentration of ice particles produced by various SIP mechanisms such as sublimation breakup, raindrop freezing, ice-ice collision breakup, and the Hallett-Mossop process as a function of temperature, averaged conditionally over only (b) convective and (c) stratiform regions. The convective and stratiform regions were identified based on criteria $|w| > 1$ and $|w| < 1$, respectively. The total ice number concentration and concentration of active INP are also displayed. All the vertical profiles shown here are averaged for the whole domain.

https://doi.org/10.5194/acp-2021-927
Preprint. Discussion started: 11 January 2022

Atmospheric Chemistry and Physics Discussions

Primary ice formation by homogeneous freezing of supercooled cloud droplets dominates the total ice budget. Among all SIP mechanisms, breakup caused by collisions between various ice particles is the most important in determining total ice number concentration. The ice production by sublimation breakup of graupel is slightly lower than homogeneous freezing. However, the contribution of ice production via sublimation breakup of dendritic ice crystals is negligible.

Figure 6b depicts the dependency on the ambient temperature of components of ice concentration from various SIP mechanisms, as well as active INPs and total ice number concentration. Each source of ice displayed is tracked with "tagging tracers" throughout the simulation. Overall, at temperatures warmer than -30ºC, the total ice number concentration is 1-2 orders of magnitude higher than the concentration of active INPs, highlighting the importance of SIP mechanisms in ice formation. At -25ºC, breakup in ice-ice collisions contributes 50% and 10% of the total ice concentration for the convective and stratiform regions, respectively. At the same temperature, in both convective and stratiform regions, sublimation breakup and raindrop freezing contribute 7% and 0.5 %, respectively.

Secondary ice formation via the HM process of rime-splintering contributes significantly to ice production at temperatures warmer than about -15 ºC (Fig. 6b), enhancing the ice concentration beyond the primary ice. In the convective region, the contribution of this process to the total ice concentration is maximum around -5ºC (about 30%). The simulated cloud droplet diameter is mostly smaller than 15 μm. It is smaller than the cloud droplet size required for the HM process to occur. AC represents the observed dependency of rime-splintering on the concentration of droplets > 24 $\mu$m. The fluctuations in CCN concentration

https://doi.org/10.5194/acp-2021-927
Preprint. Discussion started: 11 January 2022


in the boundary layer can result in larger cloud droplet diameters in some parts of the cloud, favouring secondary ice formation via the HM process.

## 5. Results from sensitivity tests about influence from PBAP

To quantify the effect of multiple types of PBAPs on cloud properties, sensitivity tests were performed by modifying the control simulation and comparing the perturbed simulations with it.

### *5.1 All PBAPs*

Simulations were performed by eliminating all PBAPs from the control ('*no-pbap'* case) and by multiplying their initial loadings at all levels by factors of 10 and 100 ('*high-pbap'* and '*very high-pbap'* cases) respectively. Comparison with the control simulation reveals the overall effect from both the CCN and IN activities of all bioaerosols combined. These factors are justified by considering the variations in PBAP concentrations in the range of about 0.1 to 30 $L^{-1}$ over North American forests (Huffman et al. 2013). An additional simulation was conducted with a 1000-fold increase in initial PBAP loading ('*ultra high-pbap*') to investigate if these unrealistically high concentrations of PBAPs could affect the ice phase in a purely hypothetical scenario.

Additional simulations were performed by removing treatment of biological IN activity in the EP ('*no-pbap INP*' case) relative to the control run. Comparison of both additional simulations against the corresponding simulations with the full change in the PBAP loadings (no-pbap and high-pbap cases) reveals the separate roles of the INP and CCN activities for

https://doi.org/10.5194/acp-2021-927
Preprint. Discussion started: 11 January 2022




the changes in biological material. Apart from these changes in PBAPs, the perturbed simulations are identical to the control run.

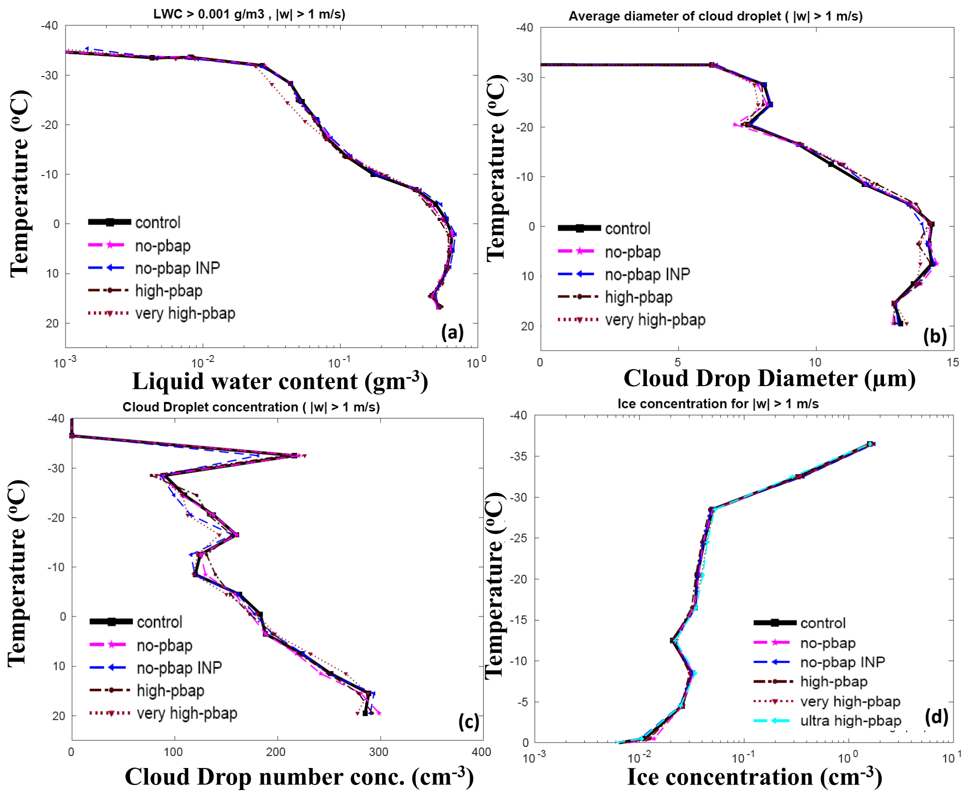


**Figure 7:** The temperature dependence of the (a) liquid water content, the (b) cloud droplet number, (c) the cloud droplet diameter, and the (d) total ice number concentration for 'control' simulation and various sensitivity runs involving a change in total PBAP number concentrations for in the convective region. The averaging conditions are mentioned at the top of each figure. The ice number concentration from the ultra high-pbap is also shown in panel d. All the vertical profiles shown here are averaged for the whole domain.

Figure 7 reveals the effects of all bioaerosols on cloud properties in the convective region (|*w*| > 1 m/s). Overall, changes in cloud microphysical properties including liquid water

https://doi.org/10.5194/acp-2021-927
Preprint. Discussion started: 11 January 2022

Atmospheric Chemistry and Physics Discussions
Open Access
EGU

content, cloud droplet size, cloud drop number concentration, ice number concentration are less sensitive to the changes in PBAPs for the convective part of the simulated clouds than the stratiform part (Figure 9). The maximum change in simulated LWC is noted in the very-high pbap simulation at -25°C and is less than 50%. The cloud droplet number and cloud drop diameter in the perturbed simulations does not differ much (< 5%) from the control run. In the convective region, changes in ice crystal number concentration due to changes in PBAPs are negligible. This includes the extreme changes in bioaerosol loading (ultra high-pbap case).

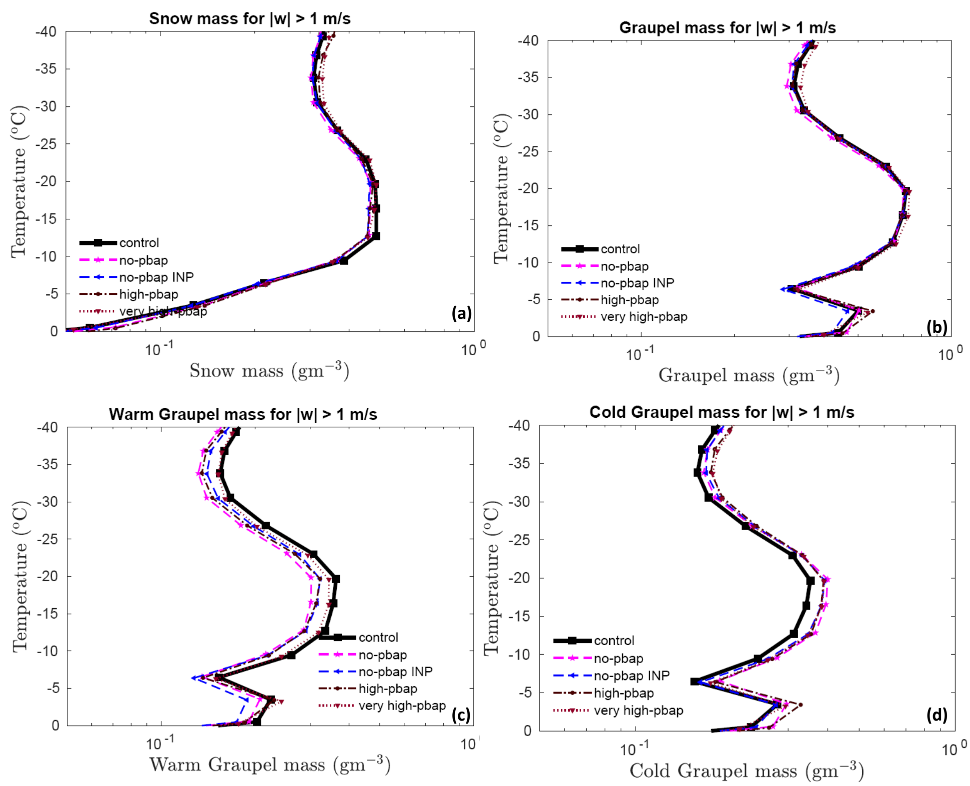


**Figure 8:** The temperature dependence of total (a) snow and (b) graupel mass for the convective region. Also shown are the (c) warm and (d) cold components of the graupel mass. All the vertical profiles shown here are averaged for the whole domain.

https://doi.org/10.5194/acp-2021-927
Preprint. Discussion started: 11 January 2022




Figure 8 shows the sensitivity of snow and graupel mass with respect to the changes in all PBAPs for the convective region. The figure also includes the sensitivities for warm and cold graupel mass to changes in PBAPs (Figures 8c and 8d). Warm graupel generation is linked to raindrop formation by collision coalescence, which then freezes to form graupel. Cold graupel is by the riming of snow through the ice crystal process. Overall, the changes in snow and graupel mass are smaller than 15% indicating their low dependence on PBAPs. The changes in PBAPs affected warm and cold components of graupel mass with a maximum change of 30% in the no-pbap run.

Figure 9 shows the corresponding effects in the stratiform region ($|w| < 1$ m/s) from all bioaerosols. The changes in warm microphysical properties as a result of changes in PBAP loadings are very small. In this part of the cloud, the ice-microphysical parameters are comparatively more sensitive to the changes in PBAPs than in the convective region. The no-pbap INP case predicted a 60% higher ice number concentration than the control run at -20ºC. This could be associated with enhanced ice formation through homogeneous nucleation since the cloud droplet number concentration at this level was slightly higher compared to the control run. At this temperature level, the changes in ice number concentrations are maximum. At the same temperature, the simulated ice crystal number concentration in the high-pbap condition is 40% lower than in the control run. Even with large increases in bioaerosol loading in the ultra high-pbap, changes in simulated ice number concentrations are less than 20% of the control run.

https://doi.org/10.5194/acp-2021-927
Preprint. Discussion started: 11 January 2022

Atmospheric Chemistry and Physics
Discussions

Figure 9e shows that at the colder temperatures ($T$ < -20ºC) homogeneous freezing aloft with downwelling of homogeneously nucleated ice dominates the ice number in all simulations. The sensitivity of ice number concentrations to PBAP loading at temperatures colder than

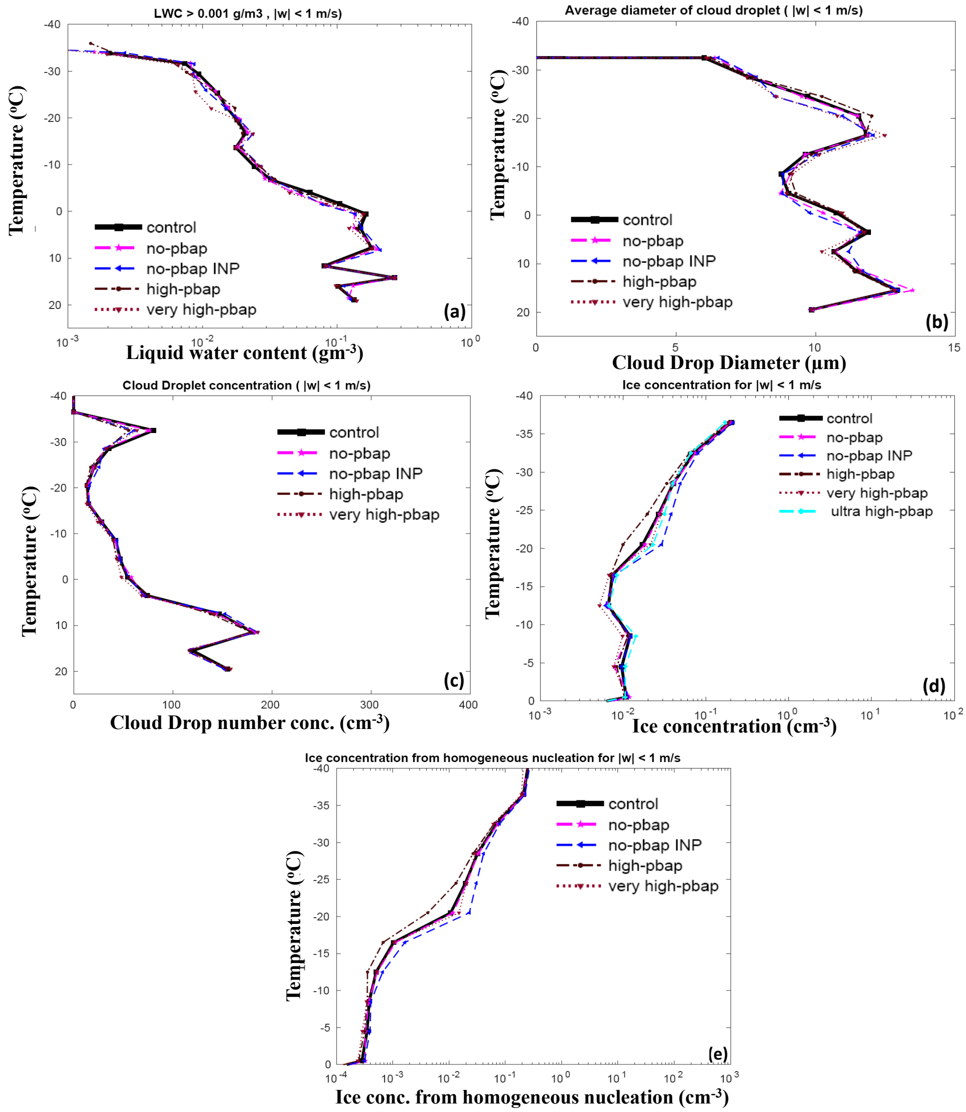


**Figure 9:** The temperature dependence of (a) the liquid water content, (b) the cloud droplet number, (c) the cloud droplet diameter, and the (d) total ice number concentration for

https://doi.org/10.5194/acp-2021-927
Preprint. Discussion started: 11 January 2022




'control' simulation and various sensitivity runs involving a change in total PBAP number concentrations for in the stratiform region. Also shown is the temperature dependence of (e) ice concentration from homogeneous freezing. The averaging conditions are mentioned at the top of each figure. The ice number concentration from ultra high-pbap is also shown in panel d. All the vertical profiles shown here are averaged for the whole domain.

-20ºC is mostly associated with homogeneously nucleated ice downwelled in the mixed-phase from above. At temperatures warmer than -15ºC the predicted ice number concentrations are less sensitive to the changes in bioaerosol loading. The biggest change was predicted for the very high-pbap case, which had a 20% lower ice number concentration than the control run. The changes in snow and graupel mass (including warm and cold components) were lower than 10% (not shown here).

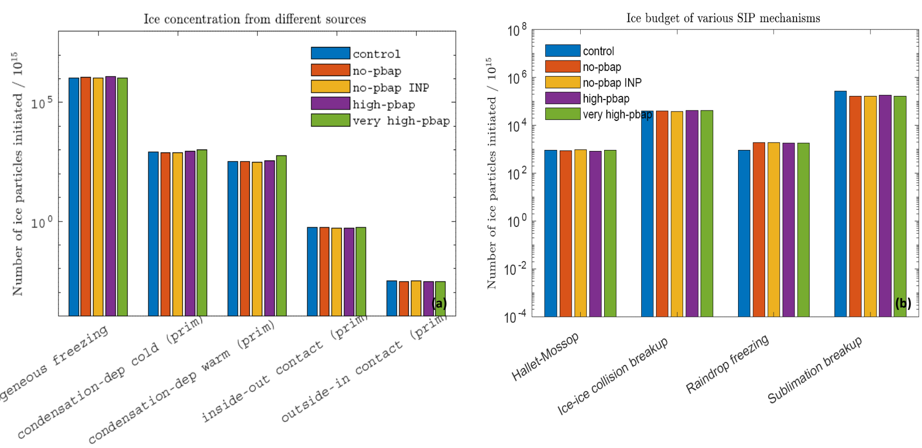


**Figure 10:** The number of ice crystals produced during the whole storm by (a) primary ice nucleation mechanisms and homogeneous freezing as well as (b) various SIP mechanisms (as shown in the legend box) per $10^{15}$ particles is shown for various sensitivity runs.

Figure 10 shows the number of ice particles generated by homogeneous nucleation, various mechanisms of primary nucleation (10a), and secondary ice production (10b) per $10^{15}$ ice particles for the entire storm. Homogeneous freezing dominates the ice production among the

https://doi.org/10.5194/acp-2021-927
Preprint. Discussion started: 11 January 2022



three broad types of ice formation mechanisms (heterogeneous and homogeneous ice nucleation, SIP). The maximum changes in ice nucleated through the primary ice mechanism are noticed for the very high-pbap case and can be attributed to the 100-fold increase in all PBAP loading. The high-pbap simulation predicted a 15% higher number of homogeneously nucleated ice than the control run. The very high-pbap cases predicted about 80% more primary ice crystals formed at temperatures warmer than -30ºC. At temperatures colder than -30ºC, this case predicted 20% more primary ice crystals than the control run.

Figure 10b shows that among SIP mechanisms, the contributions of ice-ice collision breakup and sublimation breakup are higher by an order of magnitude than the HM process and raindrop fragmentation. However, the budget analysis (not shown in the plot) showed that about 75% of the fragments associated with sublimation breakup are prone to evaporation, making ice-ice collision breakup a major SIP mechanism. The estimated ice enhancement ratio, which is a ratio between the number concentrations of total ice (excluding homogeneous nucleation) and primary ice, is two orders of magnitude which indicates the importance of SIP mechanisms. The budget analysis shows that overall, the perturbations in bioaerosols resulted in very small changes (with maximum change < 50%) in ice generated by SIP mechanisms.

https://doi.org/10.5194/acp-2021-927
Preprint. Discussion started: 11 January 2022

Atmospheric Chemistry and Physics Discussions

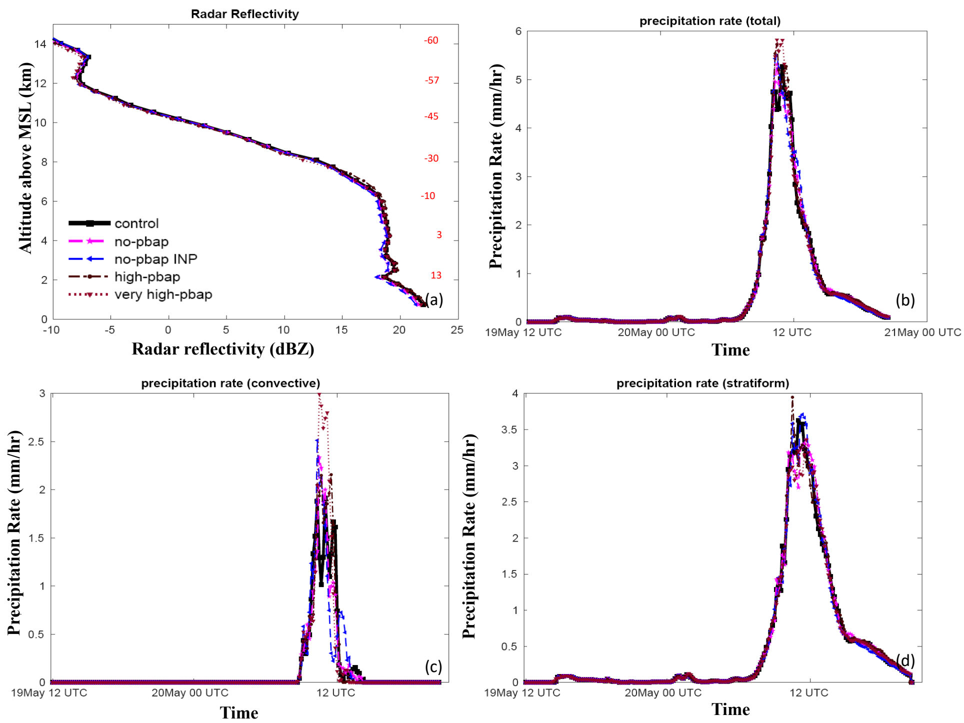


**Figure 11:** The vertical profiles of (a) radar reflectivity are shown for simulations involving changes in PBAPs. (b)The temporal evolution of the total surface precipitation rate averaged over the domain is also shown. The time series of surface precipitation rate averaged over the domain is also shown separately for (c) convective and (d) stratiform regions. All the vertical profiles shown here are averaged for the whole domain.

Figure 11a shows the effects of PBAPs on the simulated radar reflectivity for the whole storm. When compared to the control run, there is no significant difference in the simulated radar reflectivity of the perturbed simulations. Figure 11b depicts the sensitivity of the total surface precipitation rate averaged over the domain to the changes in total PBAPs. Overall, PBAPs have a minimal effect on surface precipitation, and it is most effective during the period when precipitation is at its highest. The peak in surface precipitation rate is boosted by about 10% in the very high-pbap cases compared to the control run. In remaining perturbed simulations, changes in surface precipitation rate are less than 5% when compared with the

https://doi.org/10.5194/acp-2021-927
Preprint. Discussion started: 11 January 2022


Atmospheric Chemistry and Physics
Discussions

control run. The contribution from the stratiform component of rain is higher in the total amount of rain (90%) as compared to the convective rain (remaining 10%) (see Fig. 11c and 11d). Convective rainfall is more sensitive to the changes in PBAPs than stratiform rainfall. The increase in PBAPs by 100-fold results in a 50% higher peak of convective rainfall rate as compared to the control run.

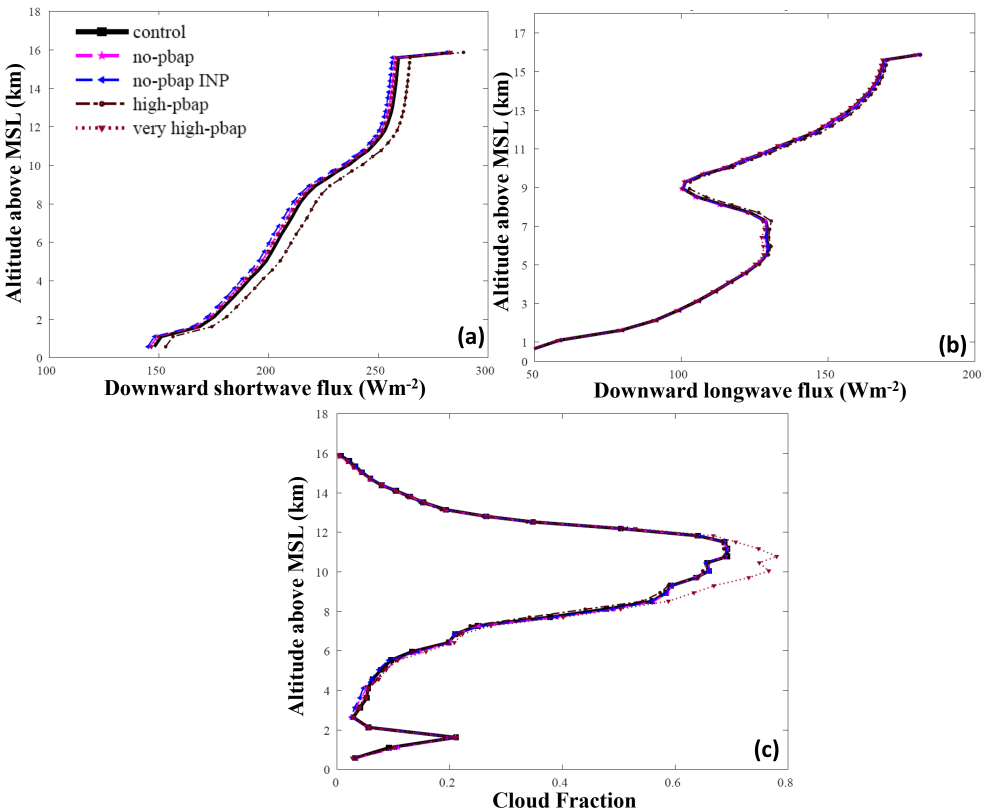


**Figure 12:** The domain averaged vertical profiles of downward components of (a) shortwave flux, (b) longwave flux, and (c) cloud fraction for various sensitivity experiments. The data shown here is an unconditional average over the whole duration and domain of each simulation. All the vertical profiles shown here are averaged for the whole domain.

https://doi.org/10.5194/acp-2021-927
Preprint. Discussion started: 11 January 2022

Atmospheric Chemistry and Physics
Discussions

Figure 12 shows the domain averaged vertical profiles of shortwave, longwave fluxes, and cloud fractions for the different sensitivity tests considered here. Among all the sensitivity runs, only the high-pbap case showed a noticeable effect on shortwave flux, which was 3% higher than the control run. The variations in longwave fluxes were less than 1%. The vertical profiles of cloud fraction show that a 100-fold increase in total PBAP results in a 10% higher cloud fraction between 8 and 12 km. The cloud fraction in other sensitivity runs was less sensitive to the changes in PBAP loadings.

*5.2 Fungi and bacteria*

To investigate the role of various PBAP groups on cloud properties, model simulations were carried out by eliminating most IN active PBAP groups including FNG and BCT from the control ('*no-fng*' and '*no-bct*' cases) run and by multiplying their initial loadings at all levels by a factor of 10 ('*high-fng*' and '*high-bct*' cases). The resulting sensitivity experiments are then compared to the control run to understand how these PBAP groups may affect cloud properties.

https://doi.org/10.5194/acp-2021-927
Preprint. Discussion started: 11 January 2022


Atmospheric Chemistry and Physics
Discussions

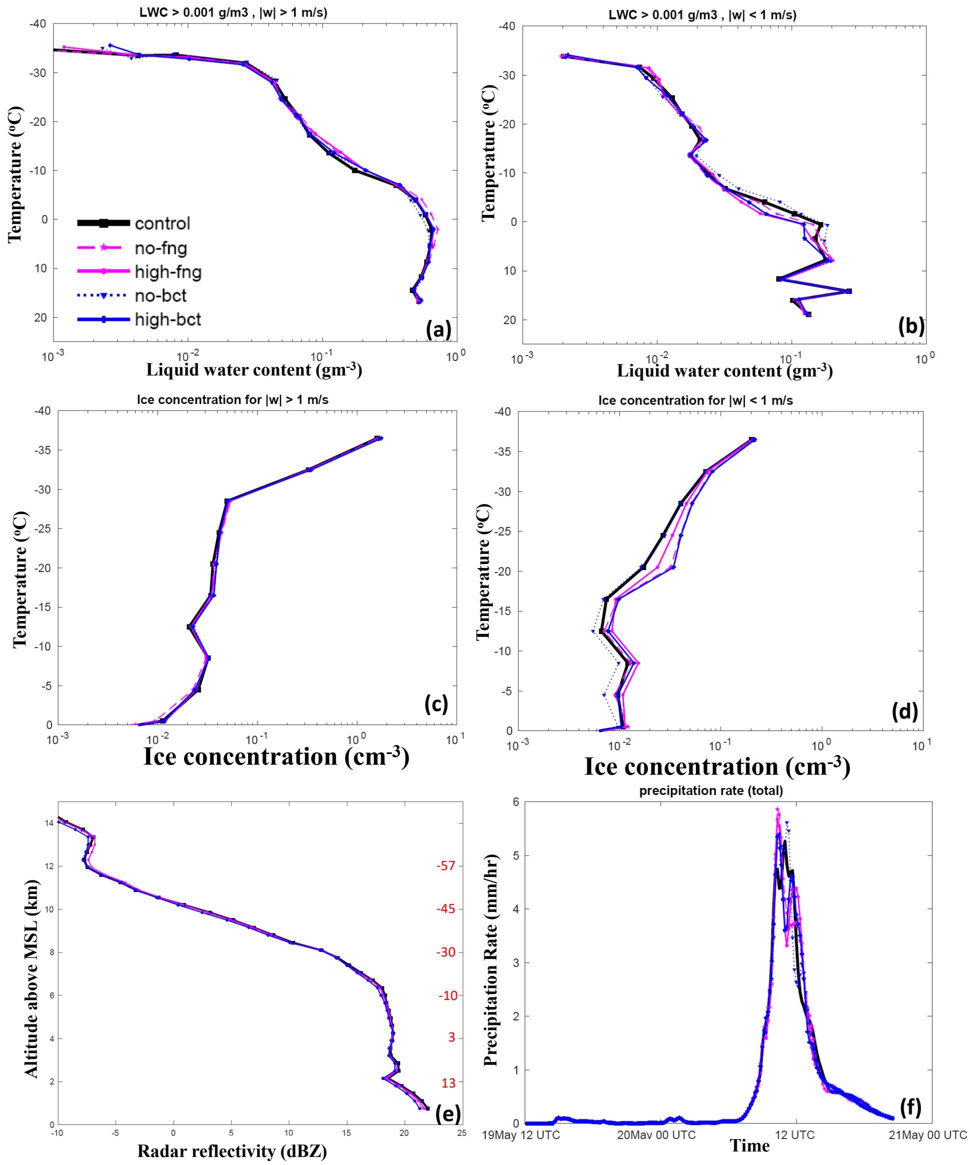


**Figure 13:** Temperature dependence of the liquid water content in (a) convective and (b) stratiform region for 'control' simulation, and various sensitivity runs involving changes in most active PBAP INPs including fungi and bacteria. Also shows is the total ice number concentration for (c) convective and (d) stratiform regions. The averaging conditions are mentioned at the top of each figure. The same simulation also shows (e) the vertical profiles of radar reflectivity. The temporal evolution of the (f) total surface precipitation rate averaged over the domain is also shown. All the vertical profiles shown here are averaged for the whole domain.

https://doi.org/10.5194/acp-2021-927
Preprint. Discussion started: 11 January 2022



Figure 13 shows the effects of these two PBAP groups on cloud parameters including LWC, ice number concentration as well as radar reflectivity, and surface precipitation for the convective region and stratiform regions. Overall, the changes in LWC due to perturbations in fungi and bacteria are very small for both convective (< 10%) and stratiform regions (< 30%). In convective regions, the perturbation in fungi and bacteria does not affect the predicted ice number concentrations with a maximum change of 5% with respect to the control run. Comparatively, in the stratiform region, the changes in ice number concentrations are more sensitive to the changes in the initial loading of fungi and bacteria. At temperatures warmer than -30ºC, the high-bct case predicted a 30% higher ice particle number concentration than the no-bct case. For fungal particles, the transition from no- to high- conditions resulted in 10% higher ice number concentration at temperatures warmer than -15ºC. At temperatures colder than -15ºC, such transition resulted in a decrease in ice number concentration by 5%.

The vertical profiles of the simulated radar reflectivity and surface precipitation rate for various sensitivity experiments involving fungi and bacteria are shown in Figures 13e and 13b respectively. The maximum differences in radar reflectivity between the no-bct and high-bct as well as no-fng and high-fng cases are smaller than 0.5 dBZ. Overall, the changes in fungal and bacterial concentrations showed little difference in the surface precipitation rate with respect to the control run (< 10%).

## 6. Results from sensitivity tests about secondary ice production

The microphysical processes of AC include several SIP mechanisms such as breakup in ice-ice collisions, raindrop freezing, sublimation breakup, etc. as mentioned in Section 3.1. Various sensitivity experiments were conducted to evaluate the role of SIP mechanisms in

https://doi.org/10.5194/acp-2021-927
Preprint. Discussion started: 11 January 2022




determining micro- and macrophysical parameters of the clouds. The SIP mechanisms, including sublimation breakup and breakup in ice-ice collisions, were turned off in the control run in the ‘no-sublimation breakup' and ‘no-collisional ice-ice breakup' simulations. In the ‘no-secondary' case, no SIP mechanisms were active.

The results from these sensitivity experiments are shown in Figure 14 for the convective region of the simulated cloud. In the no-secondary and no-collisional ice-ice breakup case, the LWC (Figure 14a) between -5 to -30ºC is higher than in the control run for both in the convective (~50%) and stratiform region (~80%). Lower ice number concentrations due to the absence of SIP mechanisms may reduce the rate of conversion of liquid to ice via mixed-phase processes, resulting in a higher LWC. The absence of all SIP mechanisms in the mixed-phase region results in a larger cloud droplet diameter (between 0.5 to 1 μm) (not shown here).

Comparing the no-SIP and control cases, the effect from the inclusion of SIP mechanisms is to increase the average ice concentration by up to half an order of magnitude at temperatures

https://doi.org/10.5194/acp-2021-927
Preprint. Discussion started: 11 January 2022


Atmospheric Chemistry and Physics
Discussions

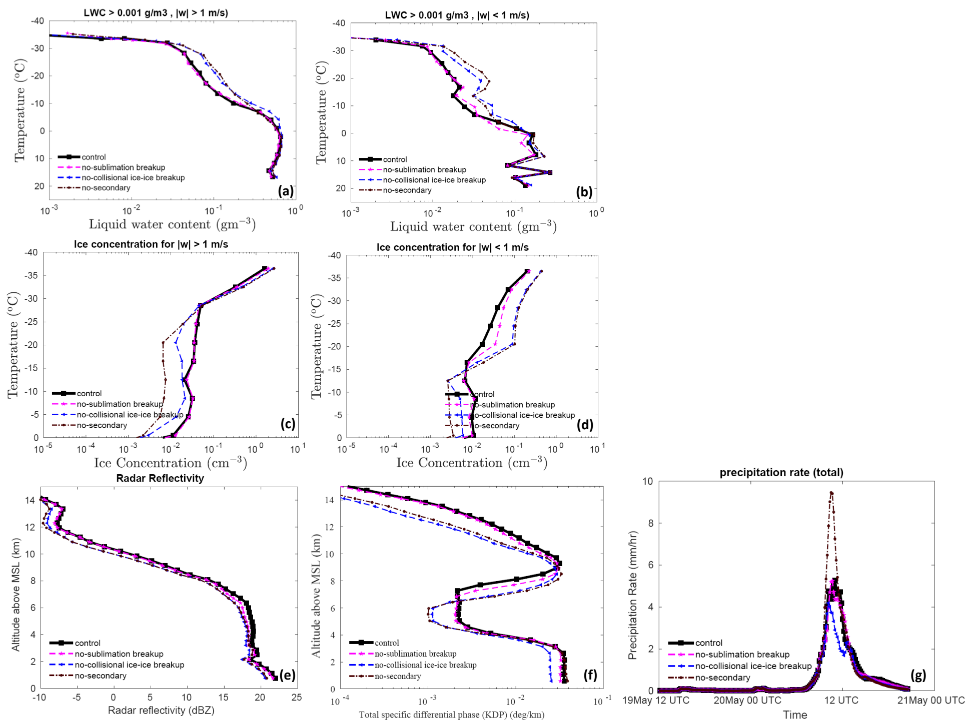


**Figure 14:** Temperature dependence of the liquid water content in (a) the convective and (b) the stratiform region for 'control' simulation and various sensitivity runs involving SIPs. The ice number concentration is also shown for the (c) convective and (d) stratiform regions. The averaging conditions are mentioned at the top of each figure. The vertical profiles of (e) radar reflectivity, (f) total specific differential phase are also shown for the same simulations. (g) The temporal evolution of the total surface precipitation rate averaged over the domain is also shown. All the vertical profiles shown here are averaged for the whole domain.

warmer than -25ºC in the stratiform region. In the convective part, the absence of any SIP increased ice number concentration by half an order of magnitude at temperatures warmer than -15ºC. At temperatures colder than this, the absence of SIP mechanisms resulted in higher ice number concentrations by a similar magnitude. The changes in ice number concentration in the no-collisional ice-ice breakup case are comparable with the no-secondary case. Compared to break up in ice-ice collisions, sublimation breakup has a lower impact (< 40%) on the total ice number concentration in both convective and stratiform regions.

https://doi.org/10.5194/acp-2021-927
Preprint. Discussion started: 11 January 2022



The changes in simulated radar reflectivity, total specific differential phase, and surface precipitation rate with SIP mechanisms are shown in Figures 14e, 14f, and 14g, respectively for the whole storm. Overall, the simulated radar reflectivity was 1 dBZ lower in the no-SIP and no-collisional ice-ice breakup case than in the control run and can be attributed to the overall increase in ice number concentration in the control run. The no-sublimation case predicted slightly higher reflectivity than the control run. The absence of all SIPs resulted in about a 100% decrease in the $K_{DP}$ at a temperature colder than -40ºC. Between -10ºC to -30ºC, the absence of no-collisional breakup and no-secondary resulted in higher $K_{DP}$ (half an order of magnitude) values than the control run. The absence of all SIP mechanisms results in a higher surface precipitation rate (75%) during the peak rainfall hour, which occurs around 11.30 UTC compared to the control run.

**7. Results about the influence of PBAP in the absence of SIP mechanisms**

Most SIP mechanisms are highly active at temperatures above -15ºC. The majority of PBAPs showed high ice nucleation activity occurs in this part of the cloud. Most of the ice concentration in this part of the cloud is determined by various SIP mechanisms. Thus, the SIP mechanisms may influence the role of PBAPs in altering cloud microphysical properties. To investigate this aspect, an additional simulation was performed by eliminating all secondary ice processes from the control run and multiplying the initial loading of all PBAP groups by a factor of 100 (the '*very high-pbap with no SIP' case*). The results of this simulation are then compared to the no-SIP case as shown in Figures 15.

https://doi.org/10.5194/acp-2021-927
Preprint. Discussion started: 11 January 2022




In the absence of any SIP mechanisms, the 100-fold increase in bioaerosols resulted in minimal effect on ice number concentration. Overall, the increase in bioaerosol loading by 100-fold resulted in less than 40% change in ice number concentration. This indicates that the ice produced by various SIP mechanisms does not alter the effect of bioaerosols on-ice number concentration in the simulated clouds. The changes in simulated radar reflectivity due to a 100-fold increase in bioaerosols are negligible (< 0.5%) (Figure 15c). The predicted surface precipitation rate difference between very high-pbap with no-secondary and no-secondary cases was lower than 5%.

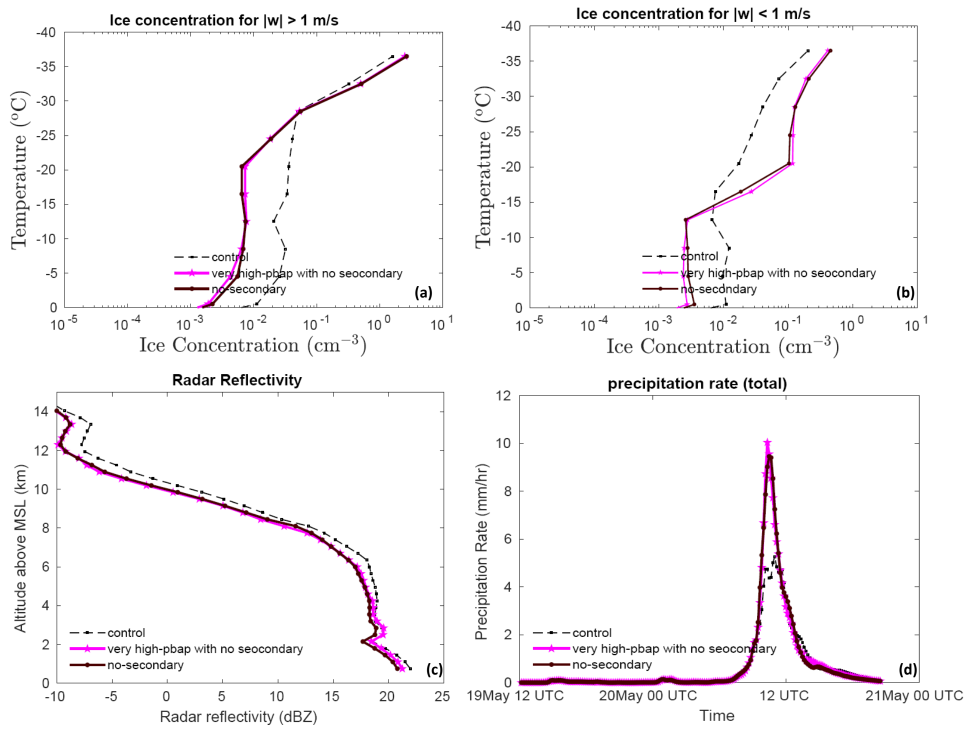


**Figure 15:** The temperature dependence of ice number concentration for the control, very high-pbap with no SIP and no-SIP simulations averaged for (a) convective and (b) stratiform regions. The (c) vertical profile of radar reflectivity and the temporal evolution of (d) surface precipitation rate is shown for the entire simulation. All the vertical profiles shown here are averaged for the whole domain. All the vertical profiles shown here are averaged for the whole domain.

https://doi.org/10.5194/acp-2021-927
Preprint. Discussion started: 11 January 2022



## 8. Summary and Conclusions

A framework describing the ice nucleation activity of five major groups of PBAPs including fungal spores, bacteria, pollen, viral particles, plant/animal detritus, algae, and their respective fragments was provided by PT21. The ice nucleation activity of these major PBAP groups in the EP was based on samples from the real atmosphere. The present study implements this EP in AC and investigates the role of these five PBAP groups as INPs in deep convective clouds. The high-resolution (2 km horizontally) simulations over a mesoscale 3D domain (80 km wide) using AC elucidate the impact of these PBAP groups on the cloud properties. A series of sensitivity experiments were conducted to test the impact of PBAP groups on cloud properties.

A mid-latitude squall line that occurred on 20 May 2011 during MC3E over the US Southern Great Plains is simulated with the model. The simulated number concentration of ice particles showed good agreement (to within about 10%) with aircraft observations for the convective clouds within the mesoscale system. The model predicted an ice number concentration slightly lower than the aircraft observation in the stratiform region by up to a factor of 3 between -10 and -16°C but agreed better at all other levels. This factor of 3 is similar to the uncertainty in the measurements due to various biases (e.g., Field et al. 2006), though it may also be related to the radar reflectivity there being too low (by about 8 dBZ). Nevertheless, all other simulated cloud microphysical parameters, radar reflectivity, and surface precipitation rate were in good agreement with aircraft and ground-based observations. This confirms that

AC adequately reproduced the warm and cold microphysical processes of the simulated squall line case.

Based on the sensitivity experiments, it can be concluded that PBAP INPs have only a limited effect on the average state of the ice phase of the simulated clouds of this mesoscale convective system. Any perturbation in the PBAP concentration resulted in changes in ice number concentration by < 5% convective region and by < 60% in the stratiform region with respect to the control run. Most of the changes in ice number concentration associated with changes in PBAPs are controlled by their effect on homogeneous nucleation.

The weakness of the simulated impact from realistic PBAP fluctuations is explicable mostly in terms of the low contribution from biological ice nucleation compared to non-biological INPs to overall ice initiation. In terms of ice nucleation efficiency and onset temperatures, each PBAP group has different ice nucleation properties. Based on vertical profiles of active INPs (Figures 5), the overall contribution of activated INPs from all PBAP groups to the total active INPs was ~1%. At -15$^{o}$C, temperature, the predicted number of active INPs from dust and black carbon were one order higher than PBAP INPs. At -30$^{o}$C, the predicted INPs from dust and black carbon were higher by one and two orders of magnitude, respectively, than PBAP INPs. Overall, this resulted in low sensitivity of the average ice phase to the changes in bioaerosol loading.

The ice production in the simulated cloud system at levels in the mixed-phase region (0 to -36 $^{o}$C) is largely controlled by various SIP mechanisms of which the most important is the breakup in ice-ice collisions. In the mixed-phase region, the total ice number concentration is

https://doi.org/10.5194/acp-2021-927
Preprint. Discussion started: 11 January 2022




1-2 orders of magnitude higher than that of active INPs. The ice production associated with SIP mechanisms is insensitive to the initial PBAP loading because SIP causes positive feedback of ice multiplication with ice fragments growing to become precipitation size particles that then fragment again. The explosive growth of ice concentrations occurs until limited by other factors. In the absence of any SIP mechanisms in the model, the effect of PBAP on the ice phase is again not significant. This indicates that SIP mechanisms were not the main reason for the limited effect of PBAPs on the ice phase. A previous study by Phillips et al. (2009) also noted an effect (by up to 4%) on surface shortwave and TOA longwave radiation flux because of changes in PBAP number concentration. In our study, the changes in PBAP loading caused smaller changes in simulated shortwave and longwave fluxes (< 3%).

Our results showed that surface precipitation is not affected significantly affected by changes in PBAPs. A tenfold increase in all PBAPs resulted in less than 10% change in peak values of surface precipitation rate. Using mesoscale model simulations, Phillips et al. (2009) reported a 10% increase in accumulated surface precipitation associated with deep convective clouds due to a 100-fold increase in biological particles. The perturbations in most active PBPAs such as fungi and bacteria showed little change in surface precipitation.

Our results showed that the perturbations in PBAPs have only a limited effect (< 50% in number and < 15% in mass) on the ice phase as well as on precipitation. This is consistent with the findings of Hummel *et al*. (2018). Based on ensemble simulations of the regional atmospheric model for Europe, they showed that the average ice crystal concentration by biological INPs is not statistically significant, implying that PBAPs play only a minor role in altering the cloud ice phase. Sesartic et al. (2012, 2013) showed that including fungi and bacteria in the global climate model leads to minor changes (< 0.5%) in ice water path, total cloud cover, and total precipitation on a global scale.

To conclude, our simulations involving various changes in SIP indicated that peak surface precipitation rate is highly sensitive (~75%) to the inclusion of SIP mechanisms. Eliminating all SIP mechanisms from the model results in a higher and much narrower peak in surface precipitation rate. However, even in the absence of SIP mechanisms, an increase in PBAP number still causes only a minor increase in precipitation because the contribution of active PBAP INPs to the total IN activity was only 1%.

***Code and data availability***: Data and the code for the empirical formulation of PBAPs are available on request by contacting the corresponding author.

***Competing interests***: The authors declare no conflict of interest

***Author Contributions:*** VJTP designed and monitored this study. SP conducted model simulation, most of the data analysis, and wrote the initial manuscript. All authors contributed to the scientific discussion and model development.

***Financial support:*** This work was completed for a sub-award (award number: 2019-26-03) to VTJP from a US Department of Energy (DoE) direct grant to the Ryzhkov at the University of Oklahoma (award number: DE-SC0018967). The first author was also supported by a past award from the Swedish Research Council ('VR'), which concerns modeling bio-aerosol effects on glaciated clouds (2015-05104) and Sweden's Innovation

https://doi.org/10.5194/acp-2021-927
Preprint. Discussion started: 11 January 2022


Agency (Vinnova; 2020-03406). Other co-authors were supported by a current award from the Swedish Research Council for Sustainable Development (FORMAS; award number 2018-01795) and US Department of Energy Atmospheric Sciences Research Program (award number: DE-SC0018932).

**References:**

Blyth AM, Latham J. 1993. Development of ice and precipitation in New Mexican summertime cumulus clouds. Q. J. R. Meteorol. Soc. 119:91–120

Carlin, J. T., Reeves, H. D., & Ryzhkov, A. V. 2021: Polarimetric Observations and Simulations of Sublimating Snow: Implications for Nowcasting, Journal of Applied Meteorology and Climatology, 60(8), 1035-1054.

Chin, M., R. B. Rood, S. J. Lin, J. F. Müller, and A. M. Thompson, 2000: Atmospheric sulfur cycle simulated in the global model GOCART: Model description and global properties. *Journal of Geophysical Research Atmospheres*, **105**, 24671–24687, https://doi.org/10.1029/2000JD900384.

Crawford, I., Bower, K. N., Choularton, T. W., Dearden, C., Crosier, J., Westbrook, C., Capes, G., Coe, H., Connolly, P. J., Dorsey, J. R., Gallagher, M. W., Williams, P., Trembath, J., Cui, Z., and Blyth, A.: Ice formation and development in aged, wintertime cumulus over the UK: observations and modelling, Atmos. Chem. Phys., 12, 4963–4985, https://doi.org/10.5194/acp-12-4963-2012, 2012.

Cui, Z., and K. S. Carslaw , 2006: Enhanced vertical transport efficiency of aerosol in convective clouds due to increases in tropospheric aerosol abundance, J. Geophys. Res., 111, D15212, doi:10.1029/2005JD006781

Deshmukh A., Vaughan T. J. Phillips, Aaron Bansemer, Sachin Patade, and Deepak Waman, 2021: New Empirical Formulation for the Sublimational Breakup of Graupel and Dendritic Snow, DOI: https://doi.org/10.1175/JAS-D-20-0275.1

Després, V. R., and Coauthors, 2012: Primary biological aerosol particles in the atmosphere: A review. *Tellus, Series B: Chemical and Physical Meteorology*, **64**, https://doi.org/10.3402/tellusb.v64i0.15598.

Fan, J, Liu, Y-C, Xu, K-M, North, K, Collis, S, Dong, X, Zhang, GJ, Chen, Q, Kollias, P, and Ghan, SJ (2015), Improving representation of convective transport for scale-aware parameterization: 1. Convection and cloud properties simulated with spectral bin and bulk microphysics. J. Geophys. Res. Atmos., 120, 3485– 3509. doi: 10.1002/2014JD022142.

https://doi.org/10.5194/acp-2021-927
Preprint. Discussion started: 11 January 2022


Atmospheric Chemistry and Physics
Discussions

Field, P. R., and A. J. Heymsfield (2015): Importance of snow to global precipitation, Geophys. Res. Lett., 42, 9512–9520,doi:10.1002/2015GL065497.

Field, P. R., Heymsfield, A. J., & Bansemer, A. (2006). Shattering and Particle Interarrival Times Measured by Optical Array Probes in Ice Clouds, Journal of Atmospheric and Oceanic Technology, 23(10), 1357-1371.

Forster, P., et al. (2007), Changes in atmospheric constituents and in radiative forcing, in Climate Change 2007: The Physical Science Basis: Contribution of Working Group I to the Fourth Assessment Report of the IPCC, edited by S. Solomon et al., pp. 131–234, Cambridge Univ. Press, New York.

Fridlind, A. M., and Coauthors, 2017: Derivation of aerosol profiles for MC3E convection studies and use in simulations of the 20 May squall line case. *Atmospheric Chemistry and Physics*, **17**, 5947–5972, https://doi.org/10.5194/acp-17-5947-2017.

Garcia, E., T. C. J. Hill, A. J. Prenni, P. J. DeMott, G. D. Franc, and S. M. Kreidenweis, 2012: Biogenic ice nuclei in boundary layer air over two US high plains agricultural regions. *Journal of Geophysical Research Atmospheres*, **117**, 1–12, https://doi.org/10.1029/2012JD018343.

Giangrande, S. E., S. Collis, A. K. Theisen, and A. Tokay, 2014: Precipitation estimation from the ARM distributed radar network during the MC3E campaign. *Journal of Applied Meteorology and Climatology*, **53**, 2130–2147, https://doi.org/10.1175/JAMC-D-13-0321.1.

Grützun, V., O. Knoth, and M. Simmel, 2008: Simulation of the influence of aerosol particle characteristics on clouds and precipitation with LM-SPECS: Model description and first results. *Atmospheric Research*, **90**, 233–242, https://doi.org/10.1016/j.atmosres.2008.03.002.

Hallett, J., and S. C. Mossop, 1974: Production of secondary ice particles during the riming process. Nature, 249, 26–28, https://doi.org/10.1038/249026a0.

Hoose, C., and O. Möhler, 2012: Heterogeneous ice nucleation on atmospheric aerosols: A review of results from laboratory experiments. *Atmospheric Chemistry and Physics*, **12**, 9817–9854, https://doi.org/10.5194/acp-12-9817-2012.

Hoose, C., J. E. Kristjánsson, and S. M. Burrows, 2010: How important is biological ice nucleation in clouds on a global scale? *Environmental Research Letters*, **5**, https://doi.org/10.1088/1748-9326/5/2/024009.

Huffman, J. A., and Coauthors, 2013: High concentrations of biological aerosol particles and ice nuclei during and after rain. *Atmospheric Chemistry and Physics*, **13**, 6151–6164, https://doi.org/10.5194/acp-13-6151-2013.

Hummel, M., C. Hoose, B. Pummer, C. Schaupp, J. Fröhlich-Nowoisky, and O. Möhler, 2018: Simulating the influence of primary biological aerosol particles on clouds by heterogeneous ice nucleation. *Atmospheric Chemistry and Physics*, **18**, 15437–15450, https://doi.org/10.5194/acp-18-15437-2018.

https://doi.org/10.5194/acp-2021-927
Preprint. Discussion started: 11 January 2022


Atmospheric Chemistry and Physics Discussions

Jensen, M. P., and Coauthors, 2016: The midlatitude continental convective clouds experiment (MC3E). *Bulletin of the American Meteorological Society*, **97**, 1667–1686, https://doi.org/10.1175/BAMS-D-14-00228.1.

Korolev, A. V., Kuznetsov, S. V., Makarov, Y. E., & Novikov, V. S. (1991). Evaluation of Measurements of Particle Size and Sample Area from Optical Array Probes, Journal of Atmospheric and Oceanic Technology, 8(4), 514-522.

Korolev, A. V., Emery, E. F., Strapp, J. W., Cober, S. G., Isaac, G. A., Wasey, M., & Marcotte, D. (2011). Small Ice Particles in Tropospheric Clouds: Fact or Artifact? Airborne Icing Instrumentation Evaluation Experiment, Bulletin of the American Meteorological Society, 92(8), 967-973

Kumjian, M. R, and K. A. Lombardo, 2017: Insights into the evolving microphysical and kinematic structure of northeastern U.S. winter storms from dual-polarization Doppler radar. Mon. Wea. Rev., 145, 1033–1061, https://doi.org/10.1175/MWR-D-15-0451.1.

Lawson, R. P., Woods, S. and Morrison, H., 2015: The microphysics of ice and precipitation 1195 development in tropical cumulus clouds, J. Atmos. Sci., 72(6), 2429–2445, 1196 doi:10.1175/JAS-D-14-0274.1, 2015.

Levin Z, Yankofsky S, Pardes D and Magal N 1987 J. Clim. Appl. Meteorol. 26 1188–97

Matus, A. V. and L'Ecuyer, T. S. (2017), The role of cloud phase in Earth's radiation budget, J. Geophys. Res. Atmos., 122, 2559– 2578, doi:10.1002/2016JD025951.

Möhler, O., and Coauthors, 2008: *Heterogeneous ice nucleation activity of bacteria: new laboratory experiments at simulated cloud conditions*. 1425–1435 pp. www.biogeosciences.net/5/1425/2008/.

Moisseev, D. N., Lautaportti, S., Tyynela, J., and Lim, S. (2015), Dual-polarization radar signatures in snowstorms: Role of snowflake aggregation, *J. Geophys. Res. Atmos.*, 120, 12644– 12655, doi:10.1002/2015JD023884.

Morris, C. E., F. Conen, J. Alex Huffman, V. Phillips, U. Pöschl, and D. C. Sands, 2014: Bioprecipitation: A feedback cycle linking Earth history, ecosystem dynamics and land use through biological ice nucleators in the atmosphere. *Global Change Biology*, **20**, 341–351, https://doi.org/10.1111/gcb.12447.

Murray, B. J., D. O'Sullivan, J. D. Atkinson, and M. E. Webb, 2012: Ice nucleation by particles immersed in supercooled cloud droplets. Chem. Soc. Rev., 41, 6519–6554, https://doi.org/ 10.1039/c2cs35200a.

Patade, S., Phillips, V. T. J., Amato, P., Bingemer, H. G., Burrows, S. M., DeMott, P. J., Goncalves, F. L. T., Knopf, D. A., Morris, C. E., Alwmark, C., Artaxo, P., Pöhlker, C., Schrod, J., & Weber, B. (2021). Empirical Formulation for Multiple Groups of Primary Biological Ice Nucleating Particles from Field Observations over Amazonia, Journal of the Atmospheric Sciences, 78(7), 2195-2220.

Phillips, V. T. J., and Coauthors, 2009: Potential impacts from biological aerosols on ensembles of continental clouds simulated numerically. *Biogeosciences*, **6**, 987–1014, https://doi.org/10.5194/bg-6-987-2009.

https://doi.org/10.5194/acp-2021-927
Preprint. Discussion started: 11 January 2022

Atmospheric Chemistry and Physics Discussions

Phillips, V. T. J., and Coauthors, 2017a: Ice multiplication by breakup in ice-ice collisions. Part II: Numerical simulations. *Journal of the Atmospheric Sciences*, **74**, 2789–2811, https://doi.org/10.1175/JAS-D-16-0223.1.

Phillips, V. T. J., and Coauthors, 2017b: Ice multiplication by breakup in ice-ice collisions. Part II: Numerical simulations. *Journal of the Atmospheric Sciences*, **74**, 2789–2811, https://doi.org/10.1175/JAS-D-16-0223.1.

Phillips, V. T. J., and Coauthors, 2020: Multiple environmental influences on the lightning of cold-based continental cumulonimbus clouds. Part I: Description and validation of model. *Journal of the Atmospheric Sciences*, **77**, 3999–4024, https://doi.org/10.1175/JAS-D-19-0200.1.

Phillips, V. T. J., J. I. Yano, and A. Khain, 2017c: Ice multiplication by breakup in ice-ice collisions. Part I: Theoretical formulation. *Journal of the Atmospheric Sciences*, **74**, 1705–1719, https://doi.org/10.1175/JAS-D-16-0224.1.

Phillips, V. T. J., P. J. Demott, C. Andronache, K. A. Pratt, K. A. Prather, R. Subramanian, and C. Twohy, 2013: Improvements to an empirical parameterization of heterogeneous ice nucleation and its comparison with observations. *Journal of the Atmospheric Sciences*, **70**, 378–409, https://doi.org/10.1175/JAS-D-12-080.1.

Phillips, V. T. J., S. Patade, 2021: Multiple Environmental Influences on the Lightning of Cold-based Continental Convection. Part II: Sensitivity Tests for its Charge Structure and Land-Ocean Contrast. *Journal of the Atmospheric Sciences*, https://doi.org/10.1175/JAS-D-20-0234.1

Phillips, V. T. J., S. Patade, J. Gutierrez, and A. Bansemer, 2018: Secondary ice production by fragmentation of freezing drops: Formulation and theory. *Journal of the Atmospheric Sciences*, **75**, 3031–3070, https://doi.org/10.1175/JAS-D-17-0190.1.

Prenni, A. J., and Coauthors, 2013: The impact of rain on ice nuclei populations at a forested site in Colorado. *Geophysical Research Letters*, **40**, 227–231, https://doi.org/10.1029/2012GL053953.

Ryzhkov, A., Pinsky, M., Pokrovsky, A., & Khain, A. (2011). Polarimetric Radar Observation Operator for a Cloud Model with Spectral Microphysics, Journal of Applied Meteorology and Climatology, 50(4), 873-894

Sesartic, A., U. Lohmann, and T. Storelvmo, 2012: Bacteria in the ECHAM5-HAM global climate model. *Atmospheric Chemistry and Physics*, **12**, 8645–8661, https://doi.org/10.5194/acp-12-8645-2012.

Sesartic, A., U. Lohmann, and T. Storelvmo, 2013: Modelling the impact of fungal spore ice nuclei on clouds and precipitation. *Environmental Research Letters*, **8**, https://doi.org/10.1088/1748-9326/8/1/014029.

Sinclair, V. A., Moisseev, D., and von Lerber, A. (2016), How dual-polarization radar observations can be used to verify model representation of secondary ice, J. Geophys. Res. Atmos., 121, 10,954– 10,970, doi:10.1002/2016JD025381.

https://doi.org/10.5194/acp-2021-927
Preprint. Discussion started: 11 January 2022




Sotiropoulou, G., Ickes, L., Nenes, A. and Ekman, A.: Ice multiplication from ice–ice collisions in the high Arctic, 2021b: sensitivity to ice habit, rimed fraction, ice type and uncertainties in the numerical description of the process, Atmos. Chem. Phys., 21, 9741–9760, 1313 doi:10.5194/acp-21-9741-2021,

Sotiropoulou, G., Vignon, E., Young, G., Morrison, H., O'Shea, S. J., Lachlan-Cope, T., Berne, A. and Nenes, A. 2021a: Secondary ice production in summer clouds over the Antarctic coast: 1308 An underappreciated process in atmospheric models, Atmos. Chem. Phys., 21(2), 755– 1309 771, doi:10.5194/acp-21-755-2021,

Spracklen, D. v., and C. L. Heald, 2014: The contribution of fungal spores and bacteria to regional and global aerosol number and ice nucleation immersion freezing rates. *Atmospheric Chemistry and Physics*, **14**, 9051–9059, https://doi.org/10.5194/acp-14-9051-2014.

Tsushima, Y., S. Emori, T.Ogura, et al., 2006: Importance of the mixed-phase cloud distribution in the control climate for assessing the response of clouds to carbon dioxide increase: a multi-model study. Clim Dyn 27, 113–126 (2006). https://doi.org/10.1007/s00382-006-0127-7.

Wilson, T., and Coauthors, 2015: A marine biogenic source of atmospheric ice-nucleating particles. Nature, 525, 234–238, https://doi.org/10.1038/nature14986.

Xie, S., Y. Zhang, S. E. Giangrande, M. P. Jensen, R. McCoy, and M. Zhang, 2014: Interactions between cumulus convection and its environment as revealed by the MC3E sounding array. *Journal of Geophysical Research*, **119**, 11,784-11,808, https://doi.org/10.1002/2014JD022011.

Zhao, X., & Liu, X. (2021). Global importance of secondary ice production. *Geophysical Research Letters*, 48, e2021GL092581. https://doi.org/10.1029/2021GL092581